© 2020. Published by The Company of Biologists Ltd | Journal of Cell Science (2020) 133, jcs237545. doi:10.1242/jcs.237545

RESEARCH ARTICLE

Regenerative responses following DNA damage – β-catenin mediates head regrowth in the planarian *Schmidtea mediterranea*

Annelies Wouters[1], Jan-Pieter Ploem[1], Sabine A. S. Langie[2,3], Tom Artois[1], Aziz Aboobaker[4] and Karen Smeets[1,*]

ABSTRACT

Pluripotent stem cells hold great potential for regenerative medicine. Increased replication and division, such is the case during regeneration, concomitantly increases the risk of adverse outcomes through the acquisition of mutations. Seeking for driving mechanisms of such outcomes, we challenged a pluripotent stem cell system during the tightly controlled regeneration process in the planarian *Schmidtea mediterranea*. Exposure to the genotoxic compound methyl methanesulfonate (MMS) revealed that despite a similar DNA-damaging effect along the anteroposterior axis of intact animals, responses differed between anterior and posterior fragments after amputation. Stem cell proliferation and differentiation proceeded successfully in the amputated heads, leading to regeneration of missing tissues. Stem cells in the amputated tails showed decreased proliferation and differentiation capacity. As a result, tails could not regenerate. Interference with the body-axis-associated component *β-catenin-1* increased regenerative success in tail fragments by stimulating proliferation at an early time point. Our results suggest that differences in the Wnt signalling gradient along the body axis modulate stem cell responses to MMS.

KEY WORDS: Stem cell, Planarian, Regeneration, DNA damage, β-catenin

INTRODUCTION

Stem cells drive the development and tissue renewal of all multicellular organisms. Characterizing their key properties is crucial for advancing regenerative medicine, and for a better understanding of misregulation that underpins diseases, such as tumorigenesis. Although stem cells are believed to have enhanced stress responses, ranging from upregulated DNA repair to rapid apoptosis (Dannenmann et al., 2015; Liu et al., 2013a; Maynard et al., 2008; Vahidi Ferdousi et al., 2014; Vitale et al., 2017), their molecular behaviour also depends strongly on the tissue environment in which they reside (Blanpain et al., 2004; Chacón-Martínez et al., 2018; DeGregori, 2017; Rompolas et al., 2013). Changes in the tissue landscape, for example during ageing, provide a permissive environment for malignant growth, while, in contrast, embryonic niches or specific micro-environmental cues are able to remodel and exert control over teratomas to produce normal tissue (Bianchi-Frias et al., 2019; Booth et al., 2011; Hendrix et al., 2007; Lan et al., 2019; McCullough et al., 1994; Mintz and Illmensee, 1975; Stoker et al., 1990).

The molecular pathways that regulate cell growth, morphogenesis and differentiation are key components of regeneration and tissue homeostasis but can also lead to tumorigenesis. During regeneration, strict control of these mechanisms leads to an orchestrated tissue regrowth rather than malignant transformation. Although there is a contrasting outcome for both processes, gene expression patterns during, for example, renal regeneration versus renal carcinoma are regulated concordantly for 77% of the studied genes (Riss et al., 2006). Another example of the commonality between both processes is the Wnt pathway, which is intimately linked with stem cell fate throughout development and regeneration but is also misregulated in multiple cancer types (Beachy et al., 2004; Clevers, 2006; Haegel et al., 1995; Heasman et al., 1994; Morin et al., 1997). A deeper understanding of the underlying mechanisms that protect stem cells against various types of cellular stress and the parameters that influence the switch between a healthy (regeneration) and malignant (cancer) cell fate is crucial for a myriad of stem cell applications.

Not coincidentally, tissues and species with a high regenerative ability, such as planarians, seem to have a lower predisposition towards chemically induced tumorigenesis (Enomoto and Farber, 1982; Farber, 1984; Okamoto, 1997; Oviedo and Beane, 2009; Pomerantz and Blau, 2013; Zilakos et al., 1996). While tumours have been reported in planarians, their incidence is low (Foster, 1963; Hall et al., 1986a,b; Plusquin et al., 2012; Schaeffer et al., 1991; Stevens et al., 2018; Van Roten et al., 2018). Planarians are known for their full-body regeneration, enabled by a large pool of adult pluripotent stem cells, called neoblasts. Neoblasts can provoke whole-body regeneration from a small fragment by altering proliferation, migration, differentiation and apoptosis patterns (Abnave et al., 2017; Pellettieri et al., 2010; Wenemoser and Reddien, 2010). Despite the high division rate of these stem cells, which they experience during regeneration as well as homeostasis, the incidence of malignancies is low and coincides with the absence of ageing (Oviedo and Beane, 2009; Plusquin et al., 2012; Sahu et al., 2017; Stevens et al., 2018; Tan et al., 2012). Whether this can be solely attributed to the abundantly present stem cells remains to be elucidated, as is the question of how signals from the surrounding niche are involved. With proven conservation of many signalling pathways, planarians are well-suited to the unravelling of stem cell responses within the complex multicellular entity of a regenerating tissue (Labbé et al., 2012; Onal et al., 2012; Resch et al., 2012; Swapna et al., 2018). Several studies in planarians have reported the formation of outgrowths or hyperproliferation by interfering with homologues of known mammalian tumour suppressors, such as the damage transducer SMG-1, the epigenetic regulator MLL3 and MLL4, the tumour suppressors PTEN and p53, and the Hippo pathway (de Sousa et al., 2018; González-Estévez et al., 2012; Mihaylova et al., 2018; Oviedo et al., 2008; Pearson and Sánchez

[1]Zoology, Biodiversity and Toxicology, Centre for Environmental Sciences, Hasselt University, 3590 Diepenbeek, Belgium. [2]Vito Health, 2400 Mol, Belgium. [3]Centre for Environmental Sciences, Hasselt University, 3590 Diepenbeek, Belgium. [4]Department of Zoology, University of Oxford, Oxford OX1 3PS, UK.

*Author for correspondence (karen.smeets@uhasselt.be)

K.S., 0000-0001-9673-8824

Received 7 August 2019; Accepted 9 February 2020

Journal of Cell Science (2020) 133, jcs237545. doi:10.1242/jcs.237545

Alvarado, 2010). As in other systems, neoblasts receive guiding instructions from their surroundings, such as the musculature, extracellular matrix and the nervous system (Cebria and Newmark, 2007; Fraguas et al., 2014; Isolani et al., 2013; Oviedo et al., 2010; Witchley et al., 2013). Recent studies have indicated that neoblasts respond differently to DNA damage depending on their location along the body axis (Peiris et al., 2016) and that interfering with the extracellular matrix can influence the development of outgrowths (Van Roten et al., 2018; Voura et al., 2017).

We have previously found that the planarian stem cell system reacts to genotoxic exposure by ceasing proliferation and activates different defence mechanisms depending on the developmental stage of the animal (Stevens et al., 2017, 2018). Here, we aim to further characterize how regenerative tissues respond to a genotoxic insult and whether tissue-associated factors influence the outcome. Adult worms were exposed to the genotoxic agent methyl methanesulfonate (MMS), subjected to amputation and monitored during regeneration. Our data indicate that DNA-damage-induced stem cell responses and the regenerative success are tissue-dependent and are affected by interfering with the body-axis-associated Wnt gradient.

RESULTS

In the current study, we aimed to determine stem cell stress responses and the associated physiological outcomes of a developing tissue after inducing DNA damage. Adult (i.e. uninjured) planarians were exposed to the DNA-alkylating compound MMS to induce DNA damage. After this period, damage responses were evaluated, and a regenerative response was provoked by amputation. Within this regenerative tissue, the progression of DNA damage, stem cell responses and regeneration efficiency were monitored over time (Fig. 1). By comparing responses in anterior and posterior body parts, and by interfering with the anterior–posterior Wnt gradient, the involvement of tissue-related factors in DNA damage responses was further investigated.

MMS exposure induces genotoxic effects throughout the entire body of adult animals

Adult worms were exposed for 7 days to 50 µM MMS, a sublethal concentration that evokes DNA damage in our model (Stevens et al., 2017, 2018). In line with previous measurements, we observed an increased amount of DNA damage (P<0.001) together with an increased amount of apoptotic cells (P<0.001), decreased stem cell proliferation [as determined by staining for phosphorylated histone H3 ($H3P^+$ cells), P<0.001], a decrease in the expression of the general stem cell marker *smedwi-1* (*smedwi-1* intensity, P<0.05) and a decrease in the expression of the early-progeny marker *NB.21.11e* (P<0.01) (Fig. 2; Fig. S1) (Stevens et al., 2018). All parameters were evaluated in different parts of the animals to screen for tissue-dependent effects; a comparison between anterior (prepharyngeal) and posterior (postpharyngeal) regions did not reveal significant differences (P>0.05).

Regenerative success varies along the body axis

The regenerative capacity of the exposed animals was evaluated by monitoring early tissue formation (blastema size) and regenerative success at 14 days post amputation (dpa) (Fig. 3A–C). After cutting the animal in front of the pharynx, creating an anterior (head) and posterior (tail) piece, blastema growth was most affected in the tail (Fig. 3B). While both fragment types had a significantly smaller blastema at 4 dpa (P<0.001), tail fragments failed to regenerate and a protruding blastema was never observed. The blastemas of the head fragments kept growing, yet remained proportionally smaller

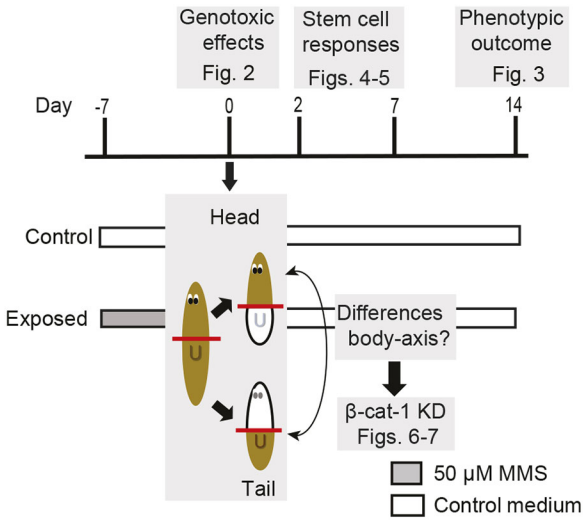

Fig. 1. Overview of the general experimental set-up. Adult (i.e. non-injured) animals were exposed to 50 µM MMS for 7 days and then amputated prepharyngeally to create an anterior (head) and posterior (tail) part. Regenerating pieces were further incubated in control medium. Initial genotoxic effects were assessed prior to the induction of regeneration (day 0). The subsequent stem cell responses were determined at an early (2 dpa) and later (7 dpa) time point, and the phenotypic outcome at 14 dpa. Responses were always compared between anterior and posterior fragment types to screen for differences along the body axis. Alternative cutting strategies, exposure or combination experiments with RNA interference (β-catenin-1) are indicated in the relevant figures.

than those in the non-exposed animals at each time point (P<0.001). The difference in blastema development between head and tail fragments was reflected in their final regenerative success at 14 dpa (Fig. 3C). This was scored as complete, aberrant or absent, based on the reappearance of missing body structures. Most heads regenerated all missing body parts, bearing a pharynx and tail, completely (63%, 26/41 animals). Manifested aberrations were the reappearance of a pharynx but not a tail (7/41) or a 'notched' tail (7/41). One animal did not regenerate. In contrast, only 19% of the tails regenerated a complete head with two eyes (8/43), 7% regenerated incompletely [a head with one centrally located eye (2/43) or no eyes (1/43)] and the majority of the tails did not regenerate at all (74%, 32/43). The body edges of the latter were smoothly aligned, indicating that wound closure took place but did not evolve further to reconstruct missing body parts. In accordance with the phenotypes, labelling the nervous system showed either connected nerve cords in the tail, a notched tail or no further development of nerve cords behind the pharynx (Fig. 3D). In tail fragments, nerve cords looped around the pharynx without the formation of cephalic ganglia (18/20 animals). The anterior marker *notum* (Petersen and Reddien, 2011) was not expressed at 3 dpa in recovering tail fragments (6/7 animals) (Fig. 3E). The posterior marker *smed-wnt-1* (Adell et al., 2009; Gurley et al., 2010; Petersen and Reddien, 2009) was present in the regenerating head fragments, but the signal was diminished as compared to that in control animals (Fig. 3E). An additional experiment suggested that the location of the cut along the anterior–posterior axis influences the final outcome, both for anterior and posterior fragments. The ability to regenerate a head increased when the cut was made more anteriorly. Likewise, the ability to regenerate a tail also increased the more posteriorly the cut was made (Fig. S2).

Anterior–posterior differences were again confirmed when excising small fragments of anterior, central (trunk) or posterior

Journal of Cell Science (2020) 133, jcs237545. doi:10.1242/jcs.237545

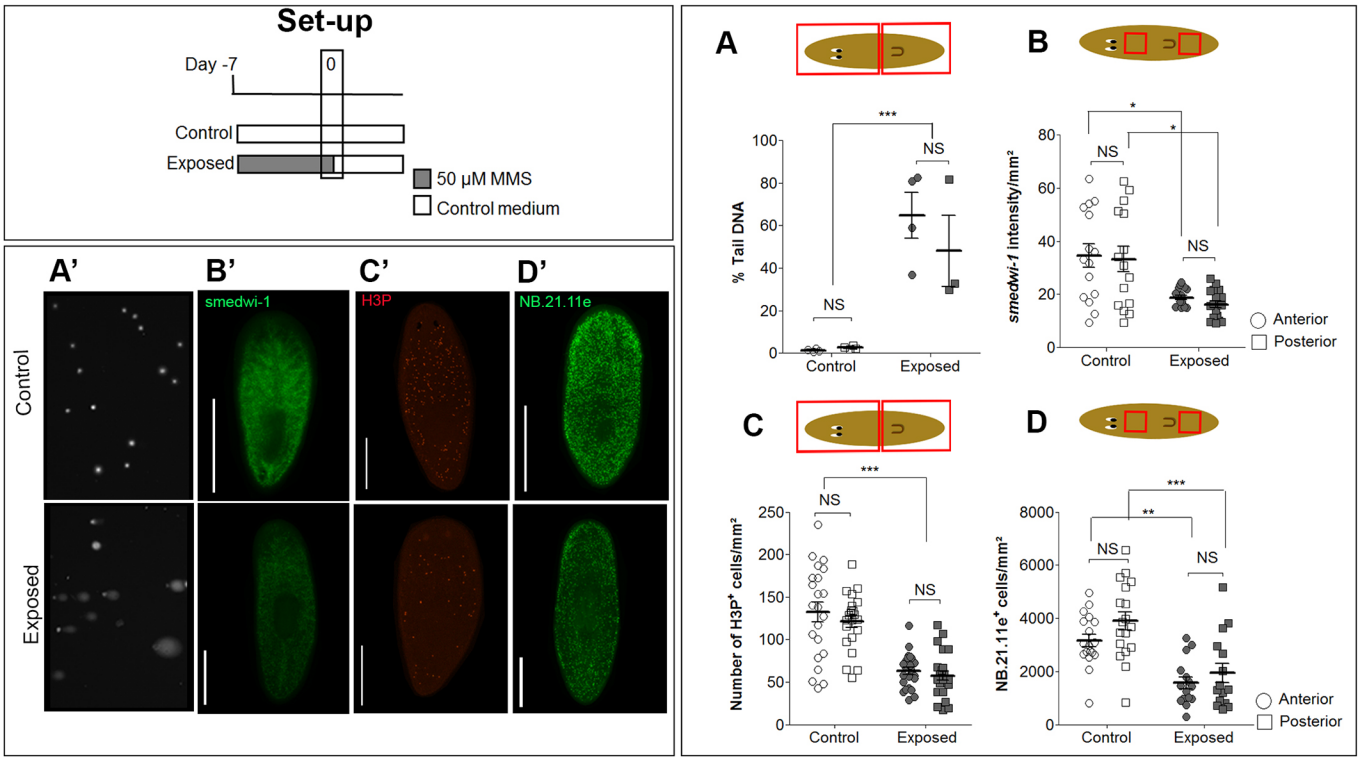

Fig. 2. Effects of MMS exposure on adult animals. An overview of the experimental procedures is summarized on the top left. (A) The mean±s.e.m. of the median percentage tail DNA of four (three for MMS posterior) replicates per condition is depicted (obtained in one experiment). Animals were cut prepharyngeally right before processing the sample. (B) The mean±s.e.m. *smedwi-1* intensity/mm². Pooled data for three independent experiments (total replicates was ≥15 per group). (C) The mean±s.e.m. absolute number of H3P$^+$ cells/mm². Pooled data of four independent experiments (total replicates was ≥22 per group). (D) The mean±s.e.m. absolute number of *NB.21.11e*$^+$ cells/mm². Pooled data of three independent experiments (total replicates was ≥15 per group). All parameters were compared between anteriorly located and posteriorly located regions, indicated by the red squares. A′–D′ display representative images for A–D. Scale bars: 500 µm. *P<0.05; **P<0.01; ***P<0.001; NS, not significant (two-way ANOVA with Tukey HSD multiple comparison for A,D; Kruskal–Wallis with pairwise Wilcoxon rank sum-test for B,C).

parts of the planarian body, with a decreasing regenerative success rate towards the posterior part of the animal (Fig. 3F). In addition, anterior-facing wounds had a lower success rate in all fragment types as compared to posterior-facing wounds. The highest regenerative success was observed in anterior fragments, which regenerated a complete head in 46% of the samples and a complete tail in 69% of the samples. The remaining samples regenerated aberrantly at both the anterior wound side (a head with one centrally located eye for 4/13 animals or an eyeless head for 1/13), and at the posterior-facing wound (notched-tail, 2/13). The posterior-facing wound of the trunks either regenerated completely (73%, 19/26 animals) or with a notched-tail (23%, 6/26); one fragment did not regenerate. Anterior regeneration was drastically lowered in these trunks (8% complete success, 2/26 animals) and in most cases was even absent (85%, 22/26). The overall success rate decreased further in the small posteriorly located fragments. While anterior regeneration was only successful in 1/12 of these posterior fragments, 6/12 were able to regenerate a tail. The mortality rate was higher in the smaller fragments (2/13 anterior fragments; 3/12 posterior), which is possibly related to their higher fragility during handling. Exposure to another alkylating compound (4-nitroquinoline 1-oxide) impaired regeneration in both head and tail fragments (Fig. S3).

Stem cell dynamics in regenerating tissue varies along the body axis

Next, we sought to characterize underlying stem cell responses leading to the observed regenerative success or failure. We assessed how the induced genotoxic effects in adult animals (Fig. 2) affected regenerative stem cell dynamics over time (Figs 4 and 5). During normal regeneration, an initial body-wide proliferation peak is followed by a local peak near the wound site at 2–3 dpa (Wenemoser and Reddien, 2010). The latter was chosen as a first time point to assess stem cell dynamics (Fig. 4). In both heads and tails, the exposure-induced DNA damage was still present at 3 dpa (P<0.001 and P<0.05, respectively) and was concomitant with a significant decrease in the expression of a general stem cell marker (*smedwi-1* intensity) at 2 dpa as compared to control animals, which was stronger in exposed tails than heads (P<0.001 versus P<0.05, Fig. 4A,B). The number of proliferative cells (H3P$^+$) in exposed head fragments was similar to that in controls (no significant difference), while their early progeny (NB.21.11e$^+$) was significantly lower (P<0.001) (Fig. 4C,D). In exposed tail fragments, both proliferation (P<0.001) and early differentiation (P<0.001) were significantly decreased as compared to non-exposed animals. Both proliferation and differentiation were significantly higher in exposed heads than in exposed tails (P<0.01 and P<0.05, respectively) (Fig. 4C,D).

At 7 dpa, no significant differences in the measured parameters were observed for exposed heads (Fig. 5A–D). In exposed tails, only the number of early progeny cells was significantly decreased (P<0.05). Since proliferation and differentiation did increase in impaired tail fragments over time, although slower than in head fragments (Fig. S5F), we assessed whether these increases could support a regenerative response at a later time point. Re-cutting

Journal of Cell Science (2020) 133, jcs237545. doi:10.1242/jcs.237545

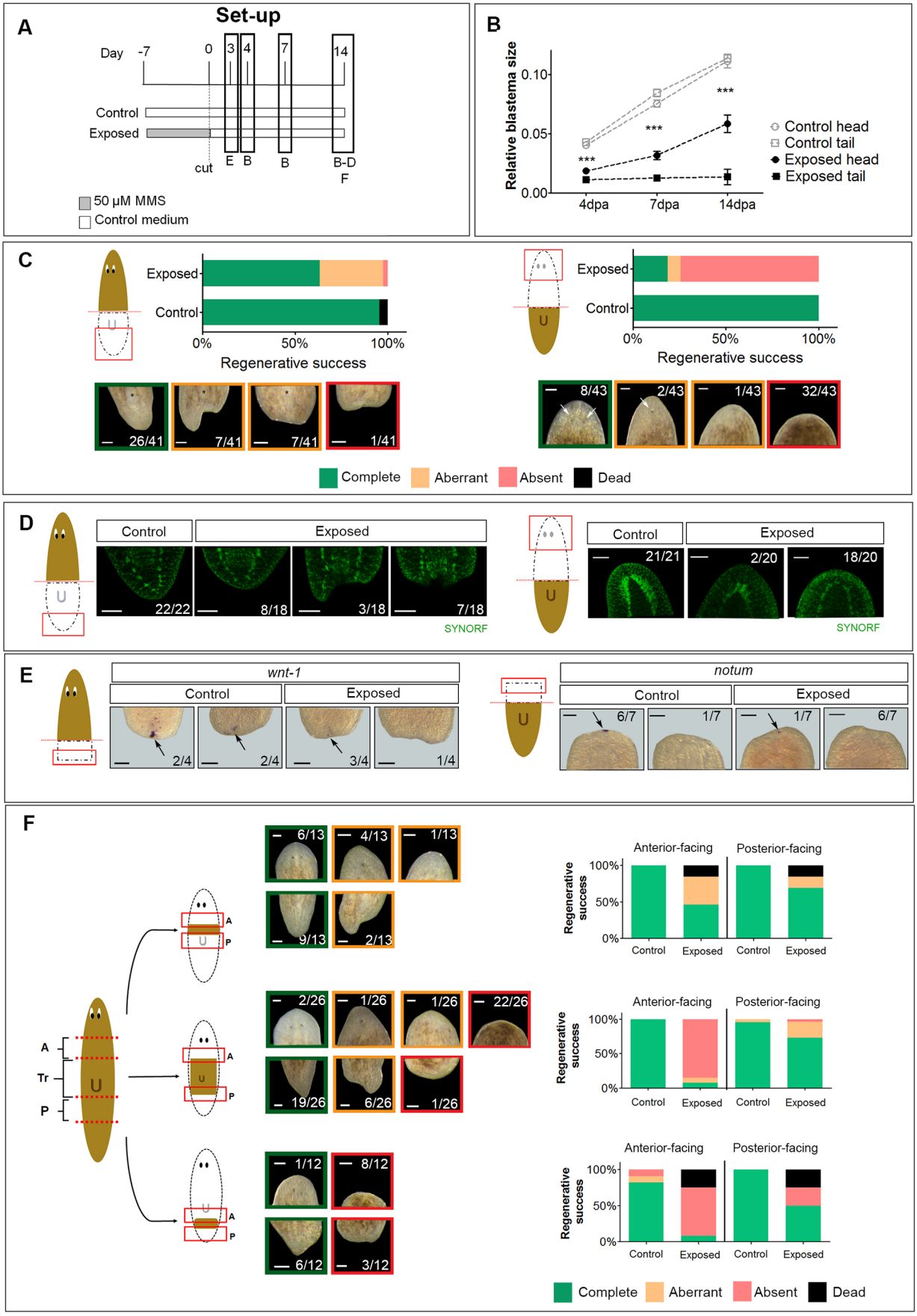

Fig. 3. See next page for legend.

Journal of Cell Science

Journal of Cell Science (2020) 133, jcs237545. doi:10.1242/jcs.237545

Fig. 3. Regenerative success of MMS-exposed animals. (A) Overview of the experimental procedures for the corresponding panel(s). (B) The average relative blastema size was determined at 4, 7 and 14 dpa. Pooled data of two (14 dpa) or three (4 and 7 dpa) experiments with a total of 13 or 19 biological replicates per group, respectively. The values represent mean ±s.e.m. ***P<0.001 (two-way ANOVA with Tukey HSD multiple comparison per time point; pairwise Wilcoxon rank sum-test at 14 dpa). Significant differences between exposed fragments and their respective control are depicted. (C) Regenerative success in exposed head and tail fragments. The percentage regenerative success is depicted and is divided into three categories, based on the reappearance of missing body structures: complete (green colour), aberrant (orange colour) or absent (red colour). For heads, the reappearance of a pharynx and a tail was assessed and was scored aberrant in case the tail was absent or notched. For tails, the reappearance of a head with two photoreceptors was assessed and was scored aberrant in case a head with no or only one eye developed. The number of biological replicates per category is depicted in a representative example. Control animals all manifested the 'complete' phenotype and are not depicted. Combined results of seven independent experiments are depicted (total number of biological replicates was ≥41 per group). The pharynx is indicated by an asterisk, and photoreceptors by an arrow. (D) Immunostaining against SYNORF1, a pan-neuronal marker, in head and tail fragments. For heads, the reappearance of nerve cords branching together in the tail tip is depicted. For tails, the reappearance of brain ganglia is depicted. The number of replicates manifesting the shown level of nerve development is shown. Combined results of three independent experiments are shown. (E) Whole-mount ISH of *wnt-1* in head fragments and *notum* in tail fragments from one independent experiment. (F) Regenerative success in smaller fragments, located anteriorly (A), centrally (Trunk, Tr) or posteriorly (P). For all fragment types, a separate analysis was performed for the anterior-facing wound (A) versus posterior-facing wound (P). For both wound types, the same categories were applied as for the head and tail pieces, scoring the reappearance of missing body structures as explained above. The number of replicates is shown in the figure and is the combined result of two (anterior and posterior pieces) or three (trunks) independent experiments with a total of minimum 11 (anterior and posterior pieces) or 23 (trunks) replicates per group. Scale bars: 100 µm.

impaired tail fragments at 7 dpa rescued regeneration completely (Fig. S4).

Similar responses are observed in continuously exposed tissue over time

When animals were continuously exposed to MMS (i.e. before and after amputation), regenerative success again decreased in tails but not in heads (Fig. S5C). Stem cell proliferation in continuously exposed heads remained significantly higher than in continuously exposed tails both in the short term (2 dpa, P<0.05) and long term (7 dpa, P<0.01) (Fig. S5D,E). Both continuously exposed heads and tails had a significantly lower amount of proliferation and differentiation compared to their respective controls 2 dpa (P<0.001, Fig. S5D). While differentiation remained significantly decreased in both fragment types at 7 dpa (P<0.001 and P<0.01, respectively), only continuously exposed heads showed a similar proliferation level as controls at that time point (no significant difference).

Independently of the treatment (before±after amputation), head and tail fragments showed increasing patterns in proliferation and differentiation over time, but both parameters increased faster in heads than tails (Fig. S5F). While proliferative responses in treated animals eventually equal the levels measured in non-exposed animals, this effect became apparent in heads at an earlier time point. Similarly, proliferation increased faster in fragments that were not continuously exposed. Control levels of early differentiation, on the other hand, were never achieved in continuously exposed animals.

A long-term follow-up experiment (up to 21 dpa) was performed to estimate the occurrence of malignant development. Abnormalities were only observed in animals that were continuously exposed to MMS before and after amputation (3% for all conditions combined; n=156) (Fig. S5B). Their incidence in regenerating anterior and posterior fragments was equal. Aberrancies manifested themselves as blister-like structures on the dorsal side of the animal but were not further characterized because of their low occurrence and fragility.

Interfering with the Wnt gradient rescues otherwise impaired tail fragments

In search for factors responsible for blocking or activating regeneration specifically in posterior fragments, we interfered with the Wnt gradient, which is known to determine and maintain the anteroposterior axis during homeostasis and regeneration (Gurley et al., 2010; Petersen and Reddien, 2011, 2009). An increasing gradient of *β-catenin-1* activity towards the posterior end determines posterior identity, while knockdown of *β-catenin-1* induces the formation of a head structure, also in posteriorly facing wounds (Gurley et al., 2008; Iglesias et al., 2008; Petersen and Reddien, 2008). The failure to regenerate a head structure in exposed tails was rescued by *β-catenin-1* knockdown (β-cat-1 KD), both phenotypically (54% developed completely, 37% aberrantly) and at the level of brain development (16/17 animals developed cephalic ganglia) (Fig. 6A,B). Eyes were nonetheless under-developed as compared to those in non-exposed animals, and their regenerated brains were significantly smaller (P<0.001). Also under continuous MMS exposure, β-cat-1-KD tails had an increased regenerative capacity (Fig. S6A). A similar rescue effect was observed after knockdown of *teashirt*, a known downstream target of β-catenin-1 (Reuter et al., 2015), confirming the involvement of Wnt signalling (Fig. 6C). When damage was induced via irradiation, a known and well-studied phenomenon in planarians (Wagner et al., 2011, 2012, Lei et al., 2016, Shiroor et al., 2019 preprint), β-cat-1 KD also ameliorated the effects of irradiation (2/3 animals), although regeneration was not rescued (Fig. S6B).

To assess the rescue effects of β-cat-1 KD on the stem cell population, stem cell-related parameters were assessed in regenerating tail fragments at 1 dpa (Fig. 7). The expression of the general stem cell marker *smedwi-1* decreased following exposure and visually increased (6/7 animals) due to β-cat-1 KD (Fig. 7A). In addition, stem cell proliferation significantly increased following β-cat-1 KD in control (P<0.05) as well as exposed (P<0.001) animals (Fig. 7B). This stimulating effect on the cell cycle was confirmed by an increased expression of *cdc23* (P<0.05 in exposed animals), a positive regulator of the G2/M progression, while the expression of *cdc73*, a negative regulator of the cell cycle, was not affected by exposure or by β-cat-1 KD (Fig. 7C).

To identify how MMS exposure and β-cat-1 KD affect specific stem cell subpopulations, the expression of neoblast subclass-associated genes was measured (Fig. 7D) (van Wolfswinkel et al., 2014). The expression of the general stem cell marker *smedwi-1* significantly decreased in response to MMS treatment (P<0.001) and increased following β-cat-1 KD (P<0.001), confirming the whole-mount observations (Fig. 7A,D). Similarly, the expression of the putative pluripotency marker *tgs-1* (Zeng et al., 2018) significantly decreased following MMS exposure and increased following β-cat-1 KD, both in control and MMS-exposed animals (P<0.001). Similar decreases following exposure and increases following β-cat-1 KD were observed for the genes associated with the sigma neoblast subclass, *soxP-1* (P<0.001) and *soxP-2* (non-significant increasing trend following KD). Also the expression of zeta subclass-associated genes (*soxP-3* and *zfp-1*) decreased

Journal of Cell Science (2020) 133, jcs237545. doi:10.1242/jcs.237545

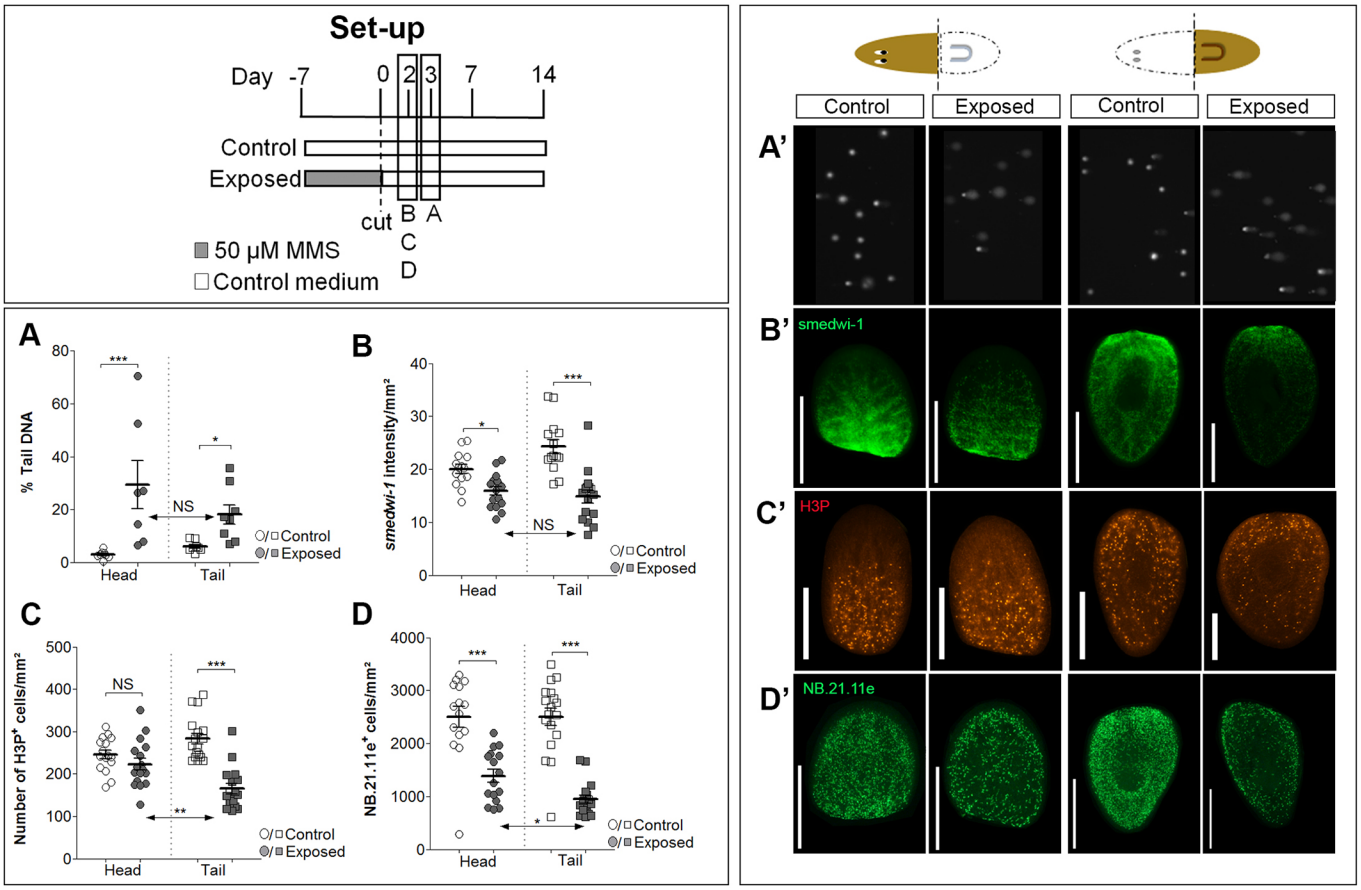

Fig. 4. DNA damage and stem cell dynamics in regenerating fragments 2 dpa. An overview of the experimental procedures is summarized in the top left corner. (A) The mean±s.e.m. of the median percentage tail DNA is depicted. Pooled data from two independent experiments (total amount of biological replicates was $n \geq 7$ per group). (B) The mean±s.e.m. *smedwi-1* intensity/mm². Pooled data of three independent experiments (total number of biological replicates was $n \geq 14$ per group). (C) The mean±s.e.m. absolute number of $H3P^+$ cells/mm². Pooled data of three independent experiments (total number of biological replicates was ≥16 per group). (D) The mean±s.e.m. absolute number of *NB.21.11e*$^+$ cells/mm². The value per sample was determined based on counting from two regions (one in front of the pharynx and one next to the pharynx). Pooled data of three independent experiments (total number of biological replicates was ≥15 per group). A′–D′ display representative images for A–D. Scale bars: 500 µm, **P*<0.05; ***P*<0.01; ****P*<0.001; NS, not significant (two-way ANOVA with Tukey HSD multiple comparison for A–C; Kruskal–Wallis with pairwise Wilcoxon rank sum-test for D). Significant differences between exposed head and tail fragments are depicted with a two-headed arrow.

following exposure (P<0.001 and P<0.05, respectively), but was not influenced by β-cat-1 KD. The expression of the gamma subclass-associated genes *gata4/5/6* and *prox1*, on the other hand, was unaffected by MMS exposure alone, but decreased in combination with β-cat-1 KD (P<0.05 and non-significant trend, respectively).

By 2 dpa, β-cat-1 KD did not affect stem cell proliferation or the number of early progeny cells (Fig. S7A,B). The amount of DNA damage was unaffected by β-cat-1 KD 3 dpa (Fig. S7C).

DISCUSSION

The inherent plasticity of stem cells confers a tissue with regenerative potential. However, an uncontrolled execution of this plasticity can cause the onset of diseases, failed wound healing or regenerative impairment (Beachy et al., 2004; Knoepfler, 2009; Ma et al., 2010; Sundaram et al., 2018). Increased lifetime, frequent replication and micro-environmental signals make stem cells vulnerable to both exogenously and endogenously induced DNA damage (Espada and Ermolaeva, 2016; Tao et al., 2015; Tomasetti and Vogelstein, 2015). Regenerative tissues and tissues in early development have the ability to restrict and tightly control cellular functioning, but alternatively can also pave the way for malignancies to arise because of the increased replication and division rates (Enomoto and Farber, 1982; Hendrix et al., 2007; Li and Ye, 2017; Ma et al., 2010; Oviedo and Beane, 2009; Pomerantz and Blau, 2013). In order to use stem cells at their full potential, it is crucial to gain more insight into how newly regenerating tissues respond to inflicted damages, preserve genomic integrity, and guard their cellular and physiological functions. Studying these processes in a regenerative model can reveal key determinants that tip the scale towards successful tissue restoration or lead to abnormal growth. Planarians have the advantage of linking underlying molecular mechanisms and stem cell behaviour to outcomes at the tissue level, such as successful development or impaired regeneration. We used the genotoxic compound MMS to challenge the planarian stem cell system and characterized (1) the regeneration potential upon induced DNA damage, (2) the underlying stem cell dynamics, (3) whether these responses led to adverse outcomes and (4) which factors influenced these outcomes. To achieve this, the regeneration process was induced via amputation after MMS exposure; stem cell responses were then monitored in the regenerating fragments over time (Fig. 1).

The alkylating agent MMS irreversibly binds to DNA strands, stalls the replication fork and disturbs normal DNA replication (Lundin et al., 2005). With stem cells being the only dividing cells

Journal of Cell Science (2020) 133, jcs237545. doi:10.1242/jcs.237545

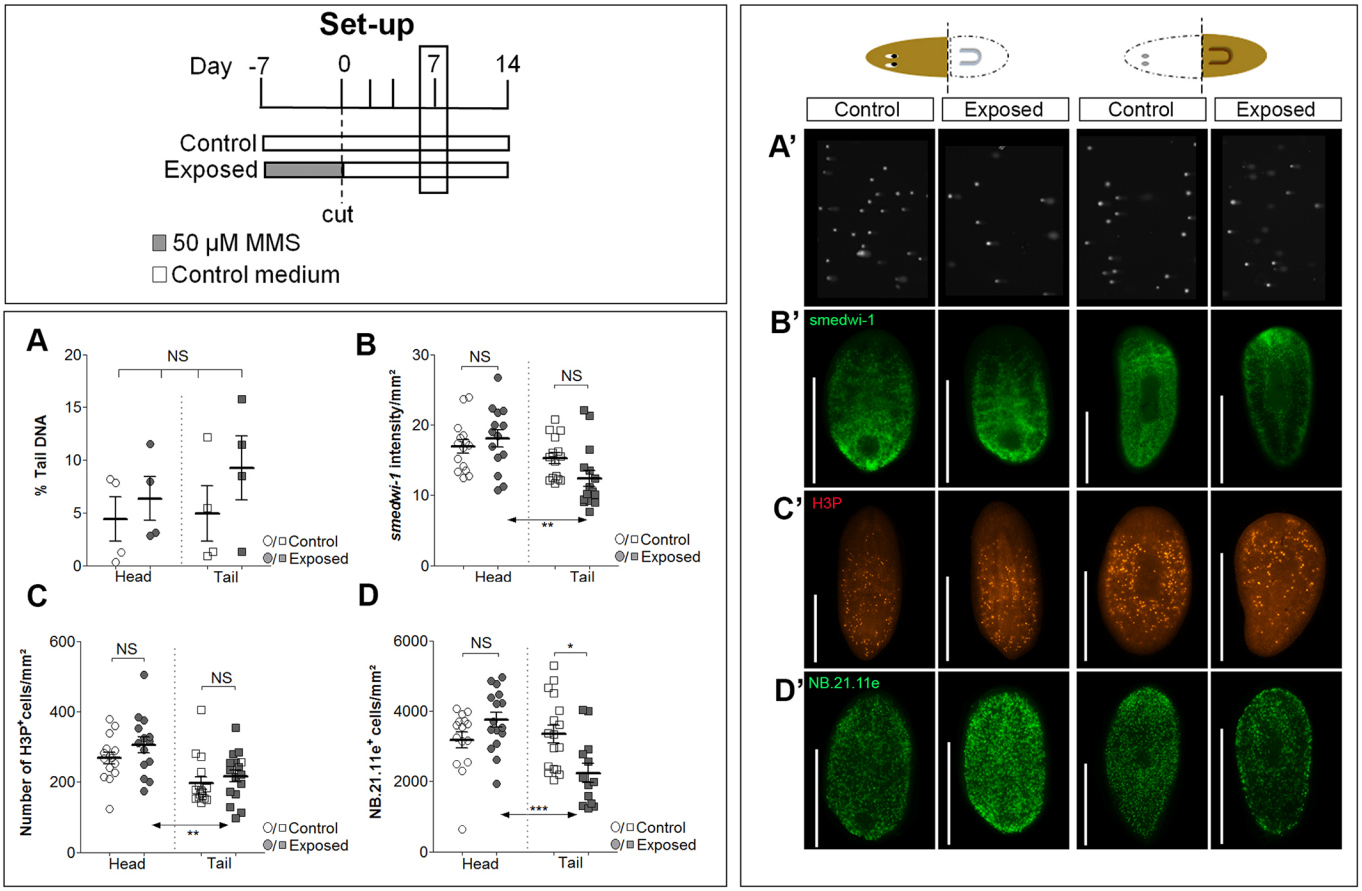

Fig. 5. DNA damage and stem cell dynamics in regenerating fragments 7 dpa. An overview of the experimental procedures is summarized in the top left corner. (A) The average mean±s.e.m. of the median percentage tail DNA of four biological replicates per group is depicted (obtained in one experiment). (B) The mean±s.e.m. *smedwi-1* intensity/mm². Pooled data of three independent experiments (total number of biological replicates was ≥14 per group). (C) The mean±s.e.m. absolute number of H3P⁺ cells/mm². Pooled data of three independent experiments (total number of biological replicates was ≥15 per group). (D) The mean±s.e.m. absolute number of *NB.21.11e*⁺ cells/mm². The value per sample was determined based on counting three regions (in front of the pharynx, next to the pharynx and behind the pharynx). Pooled data of three independent experiments (total number of biological replicates was ≥13 per group). A′–D′ display representative images for A–D. Scale bars: 500 µm, **P*<0.05; ***P*<0.01; ****P*<0.001; NS, not significant (two-way ANOVA with Tukey HSD multiple comparison). Significant differences between exposed head and tail fragments are depicted with a two-headed arrow.

in planarians, stem cell cycling was affected by the increased amount of DNA damage in our set-up (Fig. 2A), probably by halting them in the S-phase (Stevens et al., 2018). As a consequence, the amount of proliferating and descending progeny cells decreased (Fig. 2C,D). The overall decrease in the expression of the general stem cell marker *smedwi-1* could be due to damage-induced cell death, although the detected increases in apoptosis can also take place in differentiated cells (Fig. 2B; Fig. S1). The observed alterations in stem cell dynamics did not result in severe phenotypic effects in adult animals. As far as could be determined, the amount of DNA damage was equal in both the anterior and posterior regions of the adult animal (Fig. 2A), as was previously also observed after *rad51* and *ubc9* knockdown (Peiris et al., 2016; Thiruvalluvan et al., 2018). Following amputation, the amount of DNA breaks decreased in both heads and tails after 3 days, and DNA damage was completely absent at 7 dpa (Figs 2A, 4A and 5A). This corresponds to a previous study in *Dugesia schubarti* describing a similar decrease in, but not the absence of, DNA breaks 24 h after an acute MMS exposure in adult animals (Guecheva et al., 2001). Also after sublethal irradiation, *smedwi-1*-positive cells repopulate and regain their mitotic activity within a similar timespan (Lei et al., 2016; Salvetti et al., 2009; Wagner et al., 2012, 2011).

In contrast to what was observed after *rad51* KD, we did not find regional differences in proliferation or differentiation responses upon MMS-induced DNA damage in adult animals (Fig. 2) (Peiris et al., 2016). However, when challenged by tissue loss, the regenerative outcome differed along the body axis as only heads were able to regenerate (Fig. 3C). We did notice a delay in the regenerative responses of these heads, exemplified by the restricted blastema size, decreased *wnt-1* expression and an initially decreased number of early progeny cells 2 dpa (Figs 3B,E and 4D). In line with the delayed, but successful, regenerative capacities, proliferative patterns were compensated at 2 dpa, followed by an increase in early differentiation at 7 dpa (Figs 4C and 5D). In tails, on the other hand, the increasing numbers of proliferating and differentiating stem cells during regeneration were insufficient to induce the formation of a blastema (Figs 3B,C, 4C,D and 5C,D; Fig. S5F). The absence of the anterior marker *notum* (Petersen and Reddien, 2011) indicates that the anterior–posterior decision does not take place in impaired tails and regenerative responses are already affected at an early time point (Fig. 3E). In general, the numbers of proliferating and differentiating cells were significantly higher in exposed heads than tails, at early and later stages of regeneration, and this was also the case when exposure continued after amputation (Figs 4C,D and 5C,D; Fig. S5D,E). This indicates that, although amputation-associated stem cell responses

Journal of Cell Science (2020) 133, jcs237545. doi:10.1242/jcs.237545

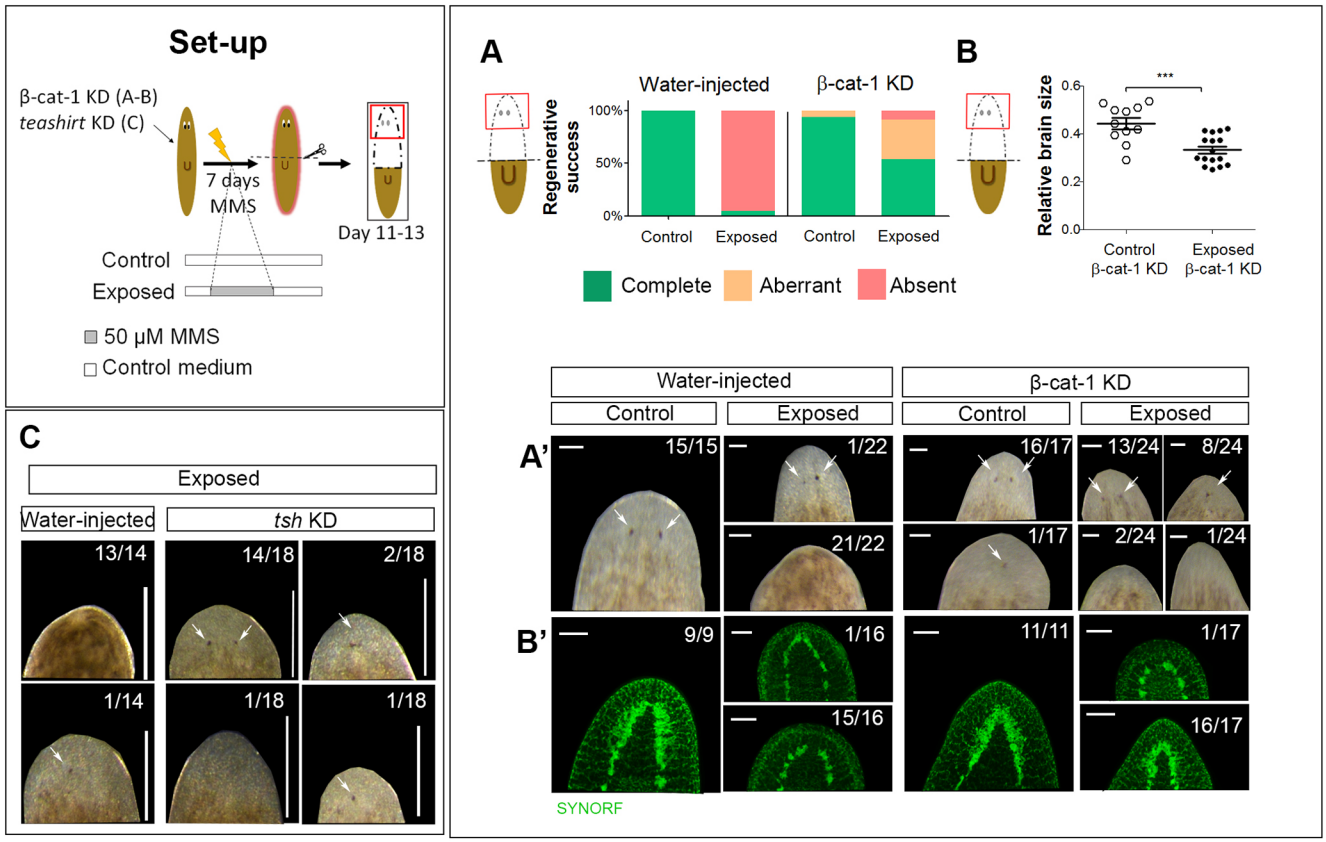

Fig. 6. Effects of *β-catenin-1* and *teashirt* knockdown in regenerating tail fragments. An overview of the experimental procedures is summarized in the top left corner. KD animals were exposed for 7 days, subsequently amputated and assessed phenotypically at 11–13 dpa. (A) Regenerative success at 11 or 13 dpa. Regenerative success was scored by assessing the reappearance of a head structure with two eyes [i.e. 'complete' (green colour, head with two eyes), 'aberrant' (orange colour, head with 1 or no eyes) or 'absent' (red colour, no outgrown blastema)]. The number of replicates per group is indicated in the figure and is the combined results of three independent experiments at 11 or 13 dpa. (B) Immunostaining against SYNORF1. The reappearance of a brain ganglion is depicted. The relative brain size of *β-catenin-1* KD animals was measured as the width of the brain relative to the width of the entire head and is the pooled data of two independent experiments. The values depicted represent mean±s.e.m. (total number of biological replicates per group was ≥11). A′ and B′ display the representative images for results depicted in the graphs in A and B. ***P<0.001 (Student's t-test). (C) Regenerative success at 11–12 dpa of *teashirt* KD animals. Data from two independent experiments. Non-exposed animals regenerated normally (11/11 *tsh* KD, 11/11 water-injected; not depicted). Scale bars: 100 µm (A′,B′); 500 µm (C).

remain active following genotoxic stress in both fragment types, their outcome depends on the tissue location (Fig. 3C; Fig. S5F).

Anterior-located amputation sites have a faster rate of head regeneration in a number of planarian species and differences in mitotic activity between body regions were described previously (Baguñà, 1976; Oviedo and Levin, 2007; Reddien and Sánchez Alvarado, 2004). Accordingly, in *S. mediterranea*, higher proliferative capacities and a higher resistance to cell death in the anterior body region have been found following *rad51* KD-induced DNA damage (Peiris et al., 2016), which is in line with our observed differences between head and tail fragments, specifically affecting anterior regeneration of posterior body parts (Figs 3–5; Fig. S5). We did not observe regional differences in stem cell responses in adult animals before amputation (Fig. 2), suggesting that regeneration-associated signals can differentially influence stem cell fate following MMS exposure (Stevens et al., 2018). To date, several (positional) cues that influence stem cell fate have been identified in planarians, with muscle cells acting as an important signalling centre for positional information (Fraguas et al., 2014; Miller and Newmark, 2012; Pirotte et al., 2015; Rossi et al., 2012; Scimone et al., 2017; Seebeck et al., 2017; Witchley et al., 2013). Neuronal signalling and the presence of the brain are often associated with a stimulating effect on stem cells (Cebria and Newmark, 2007; Peiris et al., 2016; Rossi et al., 2012), but we found no significant differences in regenerative success rates in smaller anterior fragments without a brain (Fig. 3F).

The Wnt pathway is one of the most important positional cues and is present in a gradient along the planarian anterior–posterior axis, decreasing its activity from tail to head and determining posterior identity (Adell et al., 2009; Gurley et al., 2008; Iglesias et al., 2008; Petersen and Reddien, 2008, 2009; Sureda-Gómez et al., 2016). The dual role of *β-catenin* is segregated in two distinct genes in planarians, and *β-catenin-1* solely functions as a positive mediator of Wnt signalling (Chai et al., 2010; Iglesias et al., 2008). By downregulating *β-catenin-1*, or its downstream target *teashirt*, we were able to induce regeneration in the impaired tail fragments (Fig. 6). This is in line with the previously reported rescue of head regeneration by *β-catenin-1* KD in *Dendrocoelum lacteum*, *Procotyla fluviatilis* and *Phagocata kawakatsui*, all species that are normally unable to regenerate anteriorly in posterior body fragments (Liu et al., 2013b; Sikes and Newmark, 2013; Umesono et al., 2013). Similar to what was found in *D. lacteum* and *P. fluviatilis*, we did not observe the presence of the anterior marker *smed-notum* in impaired (non-KD) tail fragments (Fig. 3E). In

Journal of Cell Science (2020) 133, jcs237545. doi:10.1242/jcs.237545

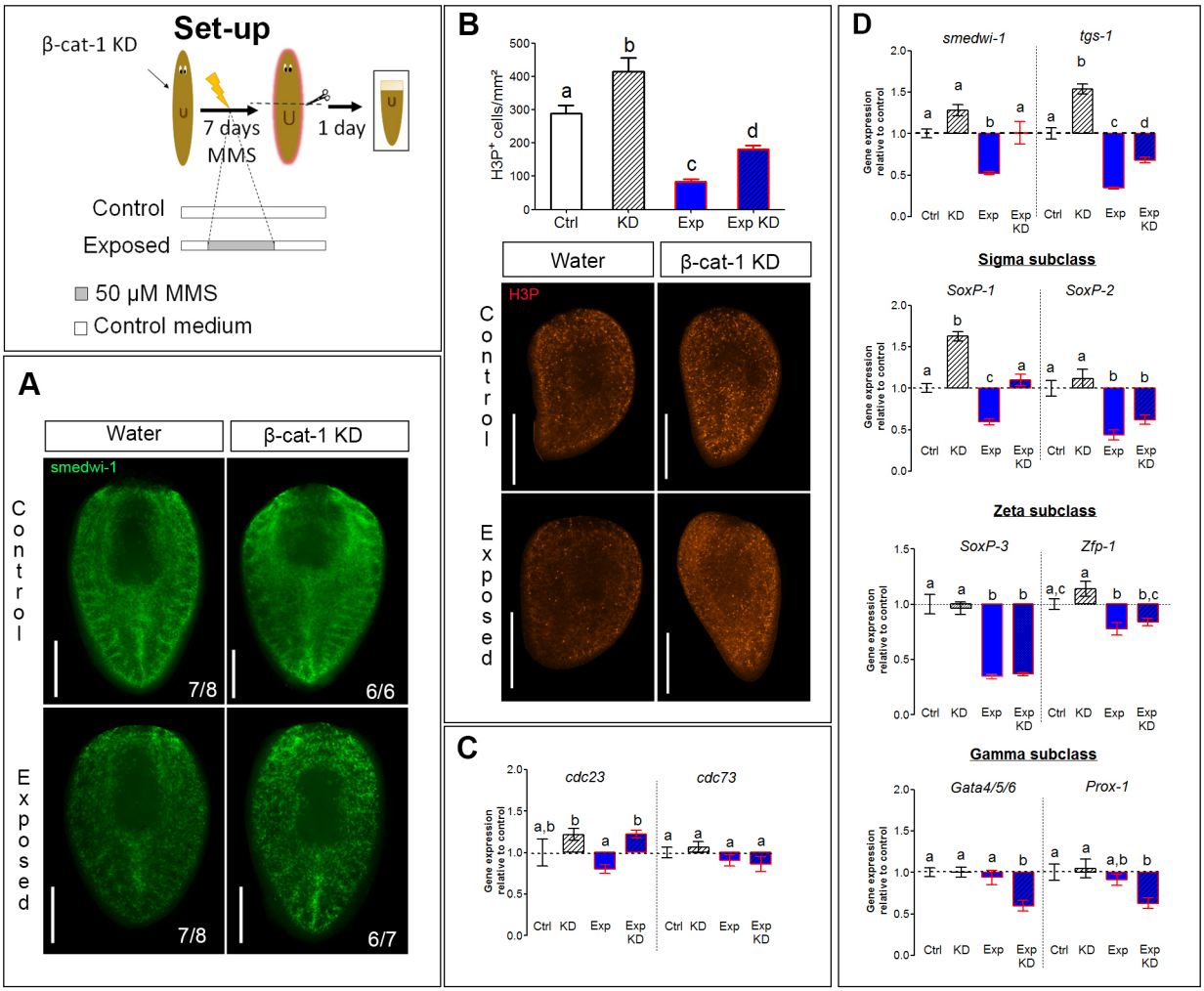

Fig. 7. Effects of *β-catenin-1* knockdown on the stem cell population. An overview of the experimental set-up is summarized in the top-left corner. β-cat-1-KD animals were exposed to MMS during 7 days, amputated prepharyngeally and sampled 1 dpa. (A) Whole-mount ISH of *smedwi-1*. The number of replicates is depicted in the right corner (one experiment). Scale bars: 500 µm. (B) The mean±s.e.m. number of $H3P^+$ cells/mm². Mean±s.e.m. of minimum of six biological replicates per condition (one experiment). A representative image per condition is depicted below. (C) Gene expression of the cell-cycle regulating genes *cdc23* and *cdc73*. (D) Gene expression of the general stem cell marker *smedwi-1*, the putative pluripotency marker *tgs-1*, sigma-subclass-associated genes (*SoxP-1* and *SoxP-2*), zeta-subclass-associated genes (*SoxP-3* and *zfp-1*) and gamma-associated genes (*Gata4*/*5*/*6* and *Prox-1*). Results in C and D are expressed as mean±s.e.m. determined relative to the non-exposed water-injected animals (Ctrl, expression set at 1) for six biological replicates per condition (five for *tgs-1*) obtained in one experiment. Significant differences between subgroups in B–D were determined via a two-way ANOVA with Tukey HSD multiple comparison testing and are depicted with a letter-code with $P<0.05$ considered significantly different. Ctrl, control water-injected; Exp, exposed, water-injected; KD, β-catenin-1 knockdown; Exp KD, exposed, β-catenin-1 knockdown.

contrast to a normal proliferative response in impaired *D. lacteum* and *P. fluviatilis* wild-type tails, we did detect a diminished proliferative response and the absence of blastema growth, indicating that the MMS exposure also affects other processes than establishing anterior or posterior fates (Figs 3B and 4C). Wnt signalling is correlated with stem cell control and with the DNA damage response pathway in other organisms (Clevers, 2006; Karimaian et al., 2017; Reya et al., 2003; Zhang et al., 2011; Zhao et al., 2018). In murine embryonic stem cells, for example, Wnt signalling was upregulated following genotoxic stress in a p53-dependent manner, thereby inhibiting differentiation (Lee et al., 2010). Murine intestinal stem cells are more sensitive to DNA damage when localized in a region with high Wnt activity and as a result apoptotic responses increased (Tao et al., 2015). A transcriptomic study in *S. mediterranea* found stem cell gene expression to be affected by β-catenin knockdown, suggesting that stem cells respond to differences in β-catenin signalling (Reuter et al., 2015). In accordance with this, we found that the expression of stem cell-associated genes increased in rescued (β-cat-1 KD) tail fragments at an early time point (1 dpa), together with an increased proliferation (Fig. 7A–D). The increased expression of a pluripotency marker (*tgs-1*) and the sigma subclass-associated *SoxP-1*, which is necessary for stem cell maintenance, suggest that β-catenin is a regulator of proliferation in tails (Wagner et al., 2012; Zeng et al., 2018). The specific increase of these genes' expression at the expense of the expression of less potent gamma subclass-associated genes is in line with this hypothesis, as it is the sigma subclass that is suggested to be the only self-renewing neoblast subclass (Lai et al., 2017). As we did not detect significant effects on the amount of DNA damage following knockdown and we found similar (although less pronounced) responses of β-cat-1 KD without MMS exposure, it is possible that β-catenin counteracts the effects of DNA damage by increasing proliferation, without having a direct role in DNA damage responses (Fig. S7C). Future research is

Journal of Cell Science (2020) 133, jcs237545. doi:10.1242/jcs.237545

needed to determine the specific function of β-catenin in response to various types of DNA damage and to reveal how DNA damage affects Wnt signalling. The fact that a downstream target of β-catenin also elicits a similar rescue effect could imply a broader role for Wnt signalling rather than β-catenin being a primary regulator. In addition, other types of DNA damage need to be assessed to fully understand the role of Wnt signalling in these processes. Inducing DNA damage via irradiation suggests that β-cat-1 KD also ameliorates irradiation effects in tail fragments (Fig. S6B). Exposure to another alkylating compound (4NQO), on the other hand, impaired regeneration in both head and tail fragments, possibly related to its stronger proliferation inhibition as compared to MMS (Fig. S3) (Stevens et al., 2017). Further research will thus be needed to determine if and how Wnt signalling functions in response to (specific types of) DNA damage.

While Wnt signalling is also active during homeostasis (Iglesias et al., 2008), we did not observe differential effects in the anterior versus posterior regions of adult (non-KD) animals (Fig. 2). β-catenin might function differently in a regenerative versus adult tissue state, in accordance with the variable role of Wnt signalling in different cell types or tissues (Clevers, 2006).

In conclusion, MMS exposure provokes equal stem cell responses in adult animals along the body axis, while stem cell responses to previously inflicted DNA damage in a regenerative context depend on their body-axis location. Anteriorly localized fragments quickly regain normal stem cell functioning and are capable of restoring missing tissue. Posterior fragments activate stem cell proliferation and differentiation processes to a lesser extent and fail to regenerate. The latter can be improved by *β-catenin-1* KD, which activates regeneration in otherwise impaired tail fragments by stimulating stem cell proliferation at an early time point. Future research will focus on further elucidating its role in planarians in a context of DNA damage in planarians.

MATERIALS AND METHODS

Experimental set-up

An asexual line of the planarian *Schmidtea mediterranea* was cultivated at 20°C in the dark in freshwater medium as described previously by Pirotte et al. (2015). Worms were fed once a week with veal liver, but were not fed during the experiments. As such, a fasting period of at least 7 days prior to measurements was taken into account to avoid food-related effects.

Worms were exposed to 50 µM methyl methanesulphonate (MMS, Sigma-Aldrich, catalogue number 129925) in various experimental set-ups in freshwater medium (1.6 mM NaCl, 1 mM $CaCl_2$, 1 mM $MgSO_4$, 0.1 mM $MgCl_2$, 0.1 mM KCl, 1.2 mM $NaHCO_3$.). In each case, medium was refreshed twice a week (every 2–3 days) with a freshly prepared MMS working solution, prepared in freshwater medium. Control animals were kept in freshwater medium and were refreshed concomitantly. Exposure was achieved in six-well plates with three or four animals per well in 3 or 4 ml of medium, respectively. Phenotypic follow-up was performed with individual worms in 1 ml of medium in a 24-well plate.

To examine how regenerative tissue recovers after a genotoxic insult, a set-up was used in which adult animals were exposed prior to the induction of regeneration (Fig. 1). Adult worms were exposed to 50 µM MMS for 7 days. The genotoxic effect of MMS was established after this initial exposure period. Regeneration was then induced with a pre-pharyngeal cut to obtain a head and tail piece. The animals were kept in freshwater medium during the regenerative phase; medium was refreshed twice a week (every 2–3 days). Samples for various measurements, as indicated below, were taken just before cutting the animals on day 0 and at 2, 3, 7 and 14 days post amputation (dpa). Alternative cutting strategies, exposures or combination experiments with RNA interference are indicated in the relevant figures and were exposed and refreshed as explained above.

Phenotypic follow-up and blastema size determination

Regenerative success was assessed by scoring the regrowth of missing body structures at 14 dpa. The reappearance of a head with two photoreceptors, a centrally located pharynx and the presence of a tail were visually inspected. Regenerative success was classified into three categories, scoring how well the missing body structures regenerated (i.e. complete, aberrant or absent). Within the considered time period, heads that have regenerated their missing body parts completely (i.e. a pharynx and tail) are scored ‘complete’. In cases where a pharynx was present but the tail did not develop completely, samples were scored ‘aberrant’. In cases where the wound closure did not develop further into the missing body structures, this was scored as ‘absent’. For tails, the regeneration of a head structure with two visible eyes was scored as ‘complete’. In cases where a head with no eyes or only one eye developed, an ‘aberrant’ score was given. If wound closure did not lead to development of the missing body structures, this was considered as ‘absent’. For the experiments where animals were cut differently (anterior–trunk–posterior), the same categories to score the presence of missing body structures were used per wound-type (anterior-facing or posterior-facing). Blastema areas were used as indication of early tissue regeneration and were measured at 4, 7 and 14 dpa. The blastema is an unpigmented region that is formed at the wound site, within which missing distal structures differentiate. The size of the blastema was measured relative to the size of the worm, determined as an average value, which was calculated based on three pictures per worm. Pictures were taken with a Nikon Ds-Ri2 digital camera mounted on a Nikon SMZ800 stereomicroscope (Nikon Instruments Inc.). The number of replicates and experiments is indicated in the respective figures.

Whole-mount fluorescent *in situ* hybridization

The expression of *smedwi-1* (general stem cell marker), *NB.21.11e* (early progeny marker that is committed to the epidermal cell lineage), *notum* (anterior pole marker) and *wnt-1* (posterior pole marker) were determined using whole-mount fluorescent or colorimetric *in situ* hybridization (ISH) (Adell et al., 2009; Eisenhoffer et al., 2008; Gurley et al., 2010; Petersen and Reddien, 2011, 2009; Reddien et al., 2005). The protocol was performed as described by King and Newmark (2013). For colorimetric ISH, development was performed using NBT/BCIP (Roche) as described by Pirotte et al. (2015). Probes were synthesized using the DIG RNA (SP6/T7) Labelling Kit (Roche) as indicated by the manufacturer, starting from a purified PCR product of the gene of interest. To obtain this, a general PCR was performed with gene-specific primers as follows: *smedwi-1* primers forward, 5′-GTGACGCAGAGAAACGGAAG-3′, reverse, 5′-TTGGATT-AGCCCCATCTTTG-3′; *NB.21.11e* primers forward, 5′-GTGATTGCGT-TCGCGTATATT-3′, reverse, 5′-ATTTATCCAGCGCGTCATATTC-3′; *notum* primers forward, 5′-CGAGTGATTTGTGGTCTGG-3′, reverse, 5′-CGTGGAGTCGTTGATTGTTG-3′; and *wnt-1* primers forward, 5′-TGA-AGGAATCAGAAAGGGTA-3′, reverse: 5′-TTGTTAGGAAAGGTCG-GTTG-3′ Samples were mounted with Immu-Mount (Thermo Fisher Scientific) and analysed with a Nikon i80 fluorescence microscope with a Nikon Ds-Ri2 digital camera using the Nikon NIS-Br software (Nikon Instruments Inc.). Because of the dense signal for *smedwi-1*, the intensity of the signal was determined using the Nikon NIS-Br software (average intensity for the region of interest). The average intensity of the entire worm or a specified region, as indicated in the figures, was used. For *NB.21.11e*, cells were counted in specified areas. In heads, one region covering the centre of the animal was used. For tails, a prepharyngeal, postpharyngeal and the region at the right side of the pharynx were used to calculate an average value per animal. For adult animals, one region located either pre- or post-pharyngeally was used as indicated in the figure. The number of replicates and independent experiments is indicated in the respective figures.

Whole-mount immunohistochemistry

The mitotic activity of stem cells was determined by immunolabelling phosphorylated histone H3 (Ser10) (H3P; Merck-Millipore, catalogue number 09-797, diluted 1:600), detected by a secondary anti-rabbit-IgG Alexa Fluor 568-conjugated antibody (Thermo Fisher Scientific, catalogue number A-11036, diluted 1:500) as described by Leynen et al. (2019). The total number of positive cells was normalized against the total body size of

the animal (determined post mounting) and was counted using the NIS-Br software (Nikon Instruments Inc.). The number of replicates and independent experiments is indicated in the respective figures.

Neuroregeneration was determined by immunolabelling synapsin (mouse anti-SYNORF1, C311, diluted 1:50, Developmental Studies Hybridoma Bank), detected by a secondary goat anti-mouse-IgG Alexa Fluor 488-conjugated antibody (Thermo Fisher Scientific, catalogue number A-1101, diluted 1:400) as described by Leynen et al. (2019). Samples were mounted with Immu-Mount (Thermo Fisher Scientific) with the ventral side upwards. Pictures were captured with a Nikon Ds-Ri2 camera mounted on a Nikon eclipse i80 fluorescence microscope and analysed using the Nikon NIS-Br software (Nikon Instruments Inc.). The presence of nerve cords and cephalic ganglia was scored visually. The relative brain size was measured as the width of the brain relative to the width of the entire head.

Comet assay

The alkaline comet assay was used to analyse the DNA-damaging effect of MMS in variable set-ups. After exposure, a stem-cell-containing fraction was obtained (from one worm per sample) using a dissociation protocol as described previously (Stevens et al., 2018), with some modifications that are mentioned below. After chemical and physical maceration, the samples were serially filtered with a 35 µm filter and a 10 µm filter (Pluriselect) to purify the fraction from larger cell types and debris. The obtained cell pellet was dissolved in 160 µl of 0.8% low-melting-point-agarose (Thermo Fisher Scientific) in phosphate-buffered saline (PBS) and immediately gelled on an agar-coated slide (1% agar in ultrapure water, Invitrogen). Each sample was made in technical duplicates (70 µl per gel). The gels were lysed overnight in lysis buffer (2.5 M NaCl, 0.1 M Na_2EDTA, 10 mM Tris, 1% Triton X-100, 10% DMSO; pH 10) at 4°C. After washing twice with cold PBS, the samples were denatured for 20 min and electrophoresis was carried out during 20 min at 4°C in electrophoresis buffer (300 mM NaOH, 1 mM Na_2EDTA, pH 13.0) at 0.95 V/cm over the platform. The buffer was continuously recirculated. Samples were neutralized first with PBS and subsequently ultrapure water, and then stained with Sybr Gold Nuclear Acid Gel Stain (Invitrogen, catalogue number S11494) for 20 min. After two washing steps with water, samples were dried and scored with a Zeiss fluorescence microscope (AxioImager.Z2, equipped with SlideFeeder X80) using the 10× objective magnification. Images were automatically captured with Metafer 5 (Metasystems). Analysis of ∼100 comets per sample (50 per technical duplicate) was performed with the comet assay IV software (Instem, Perceptive Instruments). Tail intensity (i.e. the percentage of intensity in the tail relative to the total intensity of the comet) was used as output. Four biological replicates per condition with two technical replicates per sample were analysed. A median value per technical duplicate was determined; the average of both technical duplicates was used per sample. The total number of samples and independent experiments is indicated in the respective figures.

RNA interference

To knockdown the expression of *β-catenin-1*, worms were injected for 3 consecutive days with a gene-specific dsRNA probe. Injection was undertaken prepharyngeally with three injections of 32.2 nl of a 1000 ng/µl dsRNA probe. The day after the final injection, the exposure period of adult worms began. The dsRNA probe was made based on a gene-specific amplified PCR product that was transcribed to dsRNA with the T7 Ribomax TM Express RNAi system kit (Promega) following the manufacturer's instructions. The control group was injected with ultrapure water following the same injection scheme. Primer sequences were: *β-catenin-1*, forward 5′-GCTGGATTGTTGGTTGAGGT-3′, reverse 5′-TGGTTGTGCATAATCG-GAGA-3′; and *teashirt*, forward 5′-ACAATGACACCGGGAAATGTT-3′, reverse: 5′-ACAGTCGCTATCAGGTTGGG-3′. The total number of samples and independent experiments is indicated in the respective figures.

Quantitative real-time PCR

Quantitative real-time PCR (qPCR) was performed as described previously (Stevens et al., 2018). The RNA was extracted from one animal per sample using a standard phenol:chloroform protocol. Snap-frozen samples were dissolved in 100 µl lysis buffer (Qiagen, catalogue number 79216) containing 1% β-mercaptoethanol. The extracted RNA was precipitated using sodium acetate and ethanol. The concentration and purity was determined spectrophotometrically with the Nanodrop ND-1000 (NanoDrop Technologies). DNA was removed with the Turbo DNA-free kit (Invitrogen, catalogue number AM1907) following the manufacturer's instructions. cDNA was prepared using the Superscript III first strand synthesis supermix for qRT-PCR (Thermo Fisher Scientific, catalogue number 11752250), diluted and measured under universal cycling conditions with an ABI PRISM 7500 platform (Thermo Fisher Scientific). The most stable reference genes were selected using geNorm analysis. Gene expression analysis was performed with the MIQE guidelines taken into account and details of the procedure are given in Table S1; primer sequences are listed in Table S2 (Bustin et al., 2009).

Statistical analysis and figure information

Statistical analysis was performed in Open Source RStudio version 1.0143 (RStudio Team, 2015). Depending on the research question, a *t*-test or two-way ANOVA with a Tukey honest significant difference (HSD) post-hoc test was used. Normality of the data was analysed with the Shapiro–Wilk test and equal variance with the Bartlett test. If normality criteria were not met, the dataset was transformed (log, sqrt, 1/x or e^x). If the normality criteria were still not met, a non-parametric Kruskal–Wallis test followed by a pairwise Wilcoxon rank sum test was used. $P<0.05$ was considered significant. Pictures were processed and assembled in Adobe Photoshop. The background of pictures was removed and replaced by a black background for better visualization.

Acknowledgements

The authors thank Natascha Steffanie and Ria Vanderspikken for their skilful technical assistance.

Competing interests

The authors declare no competing or financial interests.

Author contributions

Conceptualization: A.W., A.A., K.S.; Methodology: A.W., A.A., K.S.; Formal analysis: A.W., K.S.; Investigation: A.W., J.-P.P.; Resources: S.A.S.L., T.A., A.A., K.S.; Writing - original draft: A.W., K.S.; Writing - review & editing: A.W., J.-P.P., S.A.S.L., T.A., A.A., K.S.; Supervision: K.S.; Project administration: K.S.; Funding acquisition: A.W., S.A.S.L., T.A., A.A., K.S.

Funding

This study was financially supported by BOF UHasselt (16N03SMEEK) and Fonds Wetenschappelijk Onderzoek (G.0B83.17N and 1522015N to A.W.). Infrastructure was funded by The European Marine Biological Resource Centre, Belgium. S.A.S.L. is the beneficiary of a post-doctoral fellowship (12L5216N) provided by Fonds Wetenschappelijk Onderzoek and Flemish institute for Technological Research. A.A. was supported by grants from the Medical Research Council (MR/M000133/1) and Biotechnology and Biological Sciences Research Council (BB/K007564/1).

Supplementary information

Supplementary information available online at
http://jcs.biologists.org/lookup/doi/10.1242/jcs.237545.supplemental

Peer review history

The peer review history is available online at
https://jcs.biologists.org/lookup/doi/10.1242/jcs.237545.reviewer-comments.pdf

References

Abnave, P., Aboukhatwa, E., Kosaka, N., Thompson, J., Hill, M. A. and Aboobaker, A. A. (2017). Epithelial-mesenchymal transition transcription factors control pluripotent adult stem cell migration in vivo in planarians. *Development* **144**, 3440-3453. doi:10.1242/dev.154971

Adell, T., Salo, E., Boutros, M. and Bartscherer, K. (2009). Smed-Evi/Wntless is required for beta-catenin-dependent and -independent processes during planarian regeneration. *Development* **136**, 905-910. doi:10.1242/dev.033761

Baguñà, J. (1976). Mitosis in the intact and regenerating planarian Dugesia mediterranea n.sp. I. Mitotic studies during growth, feeding and starvation. *J. Exp. Zool.* **195**, 53-64. doi:10.1002/jez.1401950106

Beachy, P. A., Karhadkar, S. S. and Berman, D. M. (2004). Tissue repair and stem cell renewal in carcinogenesis. *Nature* **432**, 324-331. doi:10.1038/nature03100

Bianchi-Frias, D., Damodarasamy, M., Hernandez, S. A., Gil da Costa, R. M., Vakar-Lopez, F., Coleman, I. M., Reed, M. J. and Nelson, P. S. (2019). The aged microenvironment influences the tumorigenic potential of malignant prostate epithelial cells. *Mol. Cancer Res.* **17**, 321-331. doi:10.1158/1541-7786.MCR-18-0522

Blanpain, C., Lowry, W. E., Geoghegan, A., Polak, L. and Fuchs, E. (2004). Self-renewal, multipotency, and the existence of two cell populations within an epithelial stem cell niche. *Cell* **118**, 635-648. doi:10.1016/j.cell.2004.08.012

Booth, B. W., Boulanger, C. A., Anderson, L. H. and Smith, G. H. (2011). The normal mammary microenvironment suppresses the tumorigenic phenotype of mouse mammary tumor virus-neu-transformed mammary tumor cells. *Oncogene* **30**, 679-689. doi:10.1038/onc.2010.439

Bustin, S. A., Benes, V., Garson, J. A., Hellemans, J., Huggett, J., Kubista, M., Mueller, R., Nolan, T., Pfaffl, M. W., Shipley, G. L. et al. (2009). The MIQE guidelines: minimum information for publication of quantitative real-time PCR experiments. *Clin. Chem.* **55**, 611-622. doi:10.1373/clinchem.2008.112797

Cebria, F. and Newmark, P. A. (2007). Morphogenesis defects are associated with abnormal nervous system regeneration following roboA RNAi in planarians. *Development* **134**, 833-837. doi:10.1242/dev.02794

Chacón-Martínez, C. A., Koester, J. and Wickström, S. A. (2018). Signaling in the stem cell niche: regulating cell fate, function and plasticity. *Development* **145**, dev165399. doi:10.1242/dev.165399

Chai, G., Ma, C., Bao, K., Zheng, L., Wang, X., Sun, Z., Salò, E., Adell, T. and Wu, W. (2010). Complete functional segregation of planarian beta-catenin-1 and -2 in mediating Wnt signaling and cell adhesion. *J. Biol. Chem.* **285**, 24120-24130. doi:10.1074/jbc.M110.113662

Clevers, H. (2006). Wnt/beta-catenin signaling in development and disease. *Cell* **127**, 469-480. doi:10.1016/j.cell.2006.10.018

Dannenmann, B., Lehle, S., Hildebrand, D. G., Kübler, A., Grondona, P., Schmid, V., Holzer, K., Fröschl, M., Essmann, F., Rothfuss, O. et al. (2015). High glutathione and glutathione peroxidase-2 levels mediate cell-type-specific DNA damage protection in human induced pluripotent stem cells. *Stem Cell Rep.* **4**, 886-898. doi:10.1016/j.stemcr.2015.04.004

de Sousa, N., Rodriguez-Esteban, G., Rojo-Laguna, J. I., Salo, E. and Adell, T. (2018). Hippo signaling controls cell cycle and restricts cell plasticity in planarians. *PLoS Biol.* **16**, e2002399. doi:10.1371/journal.pbio.2002399

DeGregori, J. (2017). Connecting cancer to its causes requires incorporation of effects on tissue microenvironments. *Cancer Res.* **77**, 6065-6068. doi:10.1158/0008-5472.CAN-17-1207

Eisenhoffer, G. T., Kang, H. and Sánchez Alvarado, A. (2008). Molecular analysis of stem cells and their descendants during cell turnover and regeneration in the planarian Schmidtea mediterranea. *Cell Stem Cell* **3**, 327-339. doi:10.1016/j.stem.2008.07.002

Enomoto, K. and Farber, E. (1982). Kinetics of phenotypic maturation of remodeling of hyperplastic nodules during liver carcinogenesis. *Cancer Res.* **42**, 2330-2335.

Espada, L. and Ermolaeva, M. A. (2016). DNA damage as a critical factor of stem cell aging and organ homeostasis. *Curr. Stem Cell Rep.* **2**, 290-298. doi:10.1007/s40778-016-0052-6

Farber, E. (1984). Pre-cancerous steps in carcinogenesis. Their physiological adaptive nature. *Biochim. Biophys. Acta* **738**, 171-180. doi:10.1016/0304-419X(83)90002-1

Foster, J. A. (1963). Induction of neoplasms in planarians with carcinogens. *Cancer Res.* **23**, 300-303.

Fraguas, S., Barberán, S., Iglesias, M., Rodríguez-Esteban, G. and Cebrià, F. (2014). egr-4, a target of EGFR signaling, is required for the formation of the brain primordia and head regeneration in planarians. *Development* **141**, 1835-1847. doi:10.1242/dev.101345

González-Estévez, C., Felix, D. A., Smith, M. D., Paps, J., Morley, S. J., James, V., Sharp, T. V. and Aboobaker, A. A. (2012). SMG-1 and mTORC1 act antagonistically to regulate response to injury and growth in planarians. *PLoS Genet.* **8**, e1002619. doi:10.1371/journal.pgen.1002619

Guecheva, T., Henriques, J. A. P. and Erdtmann, B. (2001). Genotoxic effects of copper sulphate in freshwater planarian in vivo, studied with the single-cell gel test (comet assay). *Mutat. Res.* **497**, 19-27. doi:10.1016/S1383-5718(01)00244-3

Gurley, K. A., Rink, J. C. and Sánchez Alvarado, A. (2008). Beta-catenin defines head versus tail identity during planarian regeneration and homeostasis. *Science* **319**, 323-327. doi:10.1126/science.1150029

Gurley, K. A., Elliott, S. A., Simakov, O., Schmidt, H. A., Holstein, T. W. and Sánchez Alvarado, A. (2010). Expression of secreted Wnt pathway components reveals unexpected complexity of the planarian amputation response. *Dev. Biol.* **347**, 24-39. doi:10.1016/j.ydbio.2010.08.007

Haegel, H., Larue, L., Ohsugi, M., Fedorov, L., Herrenknecht, K. and Kemler, R. (1995). Lack of beta-catenin affects mouse development at gastrulation. *Development* **121**, 3529-3537.

Hall, F., Morita, M. and Best, J. B. (1986a). Neoplastic transformation in the planarian: I. Cocarcinogenesis and histopathology. *J. Exp. Zool.* **240**, 211-227. doi:10.1002/jez.1402400209

Hall, F., Morita, M. and Best, J. B. (1986b). Neoplastic transformation in the planarian: II. Ultrastructure of malignant reticuloma. *J. Exp. Zool.* **240**, 229-244. doi:10.1002/jez.1402400210

Heasman, J., Crawford, A., Goldstone, K., Garner-Hamrick, P., Gumbiner, B., McCrea, P., Kintner, C., Noro, C. Y. and Wylie, C. (1994). Overexpression of cadherins and underexpression of beta-catenin inhibit dorsal mesoderm induction in early Xenopus embryos. *Cell* **79**, 791-803. doi:10.1016/0092-8674(94)90069-8

Hendrix, M. J. C., Seftor, E. A., Seftor, R. E. B., Kasemeier-Kulesa, J., Kulesa, P. M. and Postovit, L.-M. (2007). Reprogramming metastatic tumour cells with embryonic microenvironments. *Nat. Rev. Cancer* **7**, 246-255. doi:10.1038/nrc2108

Iglesias, M., Gomez-Skarmeta, J. L., Salo, E. and Adell, T. (2008). Silencing of Smed-betacatenin1 generates radial-like hypercephalized planarians. *Development* **135**, 1215-1221. doi:10.1242/dev.020289

Isolani, M. E., Abril, J. F., Saló, E., Deri, P., Bianucci, A. M. and Batistoni, R. (2013). Planarians as a model to assess in vivo the role of matrix metalloproteinase genes during homeostasis and regeneration. *PLoS ONE* **8**, e55649. doi:10.1371/journal.pone.0055649

Karimaian, A., Majidinia, M., Bannazadeh Baghi, H. and Yousefi, B. (2017). The crosstalk between Wnt/beta-catenin signaling pathway with DNA damage response and oxidative stress: implications in cancer therapy. *DNA Repair* **51**, 14-19. doi:10.1016/j.dnarep.2017.01.003

King, R. S. and Newmark, P. A. (2013). In situ hybridization protocol for enhanced detection of gene expression in the planarian Schmidtea mediterranea. *BMC Dev. Biol.* **13**, 8. doi:10.1186/1471-213X-13-8

Knoepfler, P. S. (2009). Deconstructing stem cell tumorigenicity: a roadmap to safe regenerative medicine. *Stem Cells* **27**, 1050-1056. doi:10.1002/stem.37

Labbé, R. M., Irimia, M., Currie, K. W., Lin, A., Zhu, S. J., Brown, D. D. R., Ross, E. J., Voisin, V., Bader, G. D., Blencowe, B. J. et al. (2012). A comparative transcriptomic analysis reveals conserved features of stem cell pluripotency in planarians and mammals. *Stem Cells* **30**, 1734-1745. doi:10.1002/stem.1144

Lai, A. G., Kosaka, N., Abnave, P., Sahu, S. and Aboobaker, A. A. (2017). The abrogation of condensin function provides independent evidence for defining the self-renewing population of pluripotent stem cells. *Dev. Biol.* **433**, 218-226. doi:10.1016/j.ydbio.2017.07.023

Lan, G., Lin, Z., Zhang, J., Liu, L., Zhang, J., Zheng, L. and Luo, Q. (2019). Notch pathway is involved in the suppression of colorectal cancer by embryonic stem cell microenvironment. *Onco Targets Ther.* **12**, 2869-2878. doi:10.2147/ott.s199046

Lee, K.-H., Li, M., Michalowski, A. M., Zhang, X., Liao, H., Chen, L., Xu, Y., Wu, X. and Huang, J. (2010). A genomewide study identifies the Wnt signaling pathway as a major target of p53 in murine embryonic stem cells. *Proc. Natl Acad. Sci. USA* **107**, 69-74. doi:10.1073/pnas.0909734107

Lei, K., Thi-Kim Vu, H., Mohan, R. D., McKinney, S. A., Seidel, C. W., Alexander, R., Gotting, K., Workman, J. L. and Sánchez Alvarado, A. (2016). Egf signaling directs neoblast repopulation by regulating asymmetric cell division in planarians. *Dev. Cell* **38**, 413-429. doi:10.1016/j.devcel.2016.07.012

Leynen, N., Van Belleghem, F. G. A. J., Wouters, A., Bove, H., Ploem, J.-P., Thijssen, E., Langie, S. A. S., Carleer, R., Ameloot, M., Artois, T. et al. (2019). In vivo toxicity assessment of silver nanoparticles in homeostatic versus regenerating planarians. *Nanotoxicology* **13**, 476-491. doi:10.1080/17435390.2018.1553252

Li, H.-M. and Ye, Z.-H. (2017). Microenvironment of liver regeneration in liver cancer. *Chin. J. Integr. Med.* **23**, 555-560. doi:10.1007/s11655-017-2806-0

Liu, J. C., Guan, X., Ryan, J. A., Rivera, A. G., Mock, C., Agarwal, V., Letai, A., Lerou, P. H. and Lahav, G. (2013a). High mitochondrial priming sensitizes hESCs to DNA-damage-induced apoptosis. *Cell Stem Cell* **13**, 483-491. doi:10.1016/j.stem.2013.07.018

Liu, S.-Y., Selck, C., Friedrich, B., Lutz, R., Vila-Farré, M., Dahl, A., Brandl, H., Lakshmanaperumal, N., Henry, I. and Rink, J. C. (2013b). Reactivating head regrowth in a regeneration-deficient planarian species. *Nature* **500**, 81-84. doi:10.1038/nature12414

Lundin, C., North, M., Erixon, K., Walters, K., Jenssen, D., Goldman, A. S. and Helleday, T. (2005). Methyl methanesulfonate (MMS) produces heat-labile DNA damage but no detectable in vivo DNA double-strand breaks. *Nucleic Acids Res.* **33**, 3799-3811. doi:10.1093/nar/gki681

Ma, Y., Zhang, P., Wang, F., Yang, J., Yang, Z. and Qin, H. (2010). The relationship between early embryo development and tumourigenesis. *J. Cell. Mol. Med.* **14**, 2697-2701. doi:10.1111/j.1582-4934.2010.01191.x

Maynard, S., Swistowska, A. M., Lee, J. W., Liu, Y., Liu, S.-T., Da Cruz, A. B., Rao, M., de Souza-Pinto, N. C., Zeng, X. and Bohr, V. A. (2008). Human embryonic stem cells have enhanced repair of multiple forms of DNA damage. *Stem Cells* **26**, 2266-2274. doi:10.1634/stemcells.2007-1041

McCullough, K. D., Coleman, W. B., Smith, G. J. and Grishan, J. W. (1994). Age-dependent regulation of the tumorigenic potential of neoplastically transformed rat liver epithelial cells by the liver microenvironment. *Cancer Res.* **54**, 3668-3671.

Mihaylova, Y., Abnave, P., Kao, D., Hughes, S., Lai, A., Jaber-Hijazi, F., Kosaka, N. and Aboobaker, A. A. (2018). Conservation of epigenetic regulation by the MLL3/4 tumour suppressor in planarian pluripotent stem cells. *Nat. Commun.* **9**, 3633. doi:10.1038/s41467-018-06092-6

Miller, C. M. and Newmark, P. A. (2012). An insulin-like peptide regulates size and adult stem cells in planarians. *Int. J. Dev. Biol.* **56**, 75-82. doi:10.1387/ijdb.113443cm

Mintz, B. and Illmensee, K. (1975). Normal genetically mosaic mice produced from malignant teratocarcinoma cells. *Proc. Natl. Acad. Sci. USA* **72**, 3585-3589. doi:10.1073/pnas.72.9.3585

Morin, P. J., Sparks, A. B., Korinek, V., Barker, N., Clevers, H., Vogelstein, B. and Kinzler, K. W. (1997). Activation of beta-catenin-Tcf signaling in colon cancer by mutations in beta-catenin or APC. *Science* **275**, 1787-1790. doi:10.1126/science.275.5307.1787

Okamoto, M. (1997). Simultaneous demonstration of lens regeneration from dorsal iris and tumour production from ventral iris in the same newt eye after carcinogen administration. *Differentiation* **61**, 285-292. doi:10.1046/j.1432-0436.1997.6150285.x

Onal, P., Grun, D., Adamidi, C., Rybak, A., Solana, J., Mastrobuoni, G., Wang, Y., Rahn, H. P., Chen, W., Kempa, S. et al. (2012). Gene expression of pluripotency determinants is conserved between mammalian and planarian stem cells. *EMBO J.* **31**, 2755-2769. doi:10.1038/emboj.2012.110

Oviedo, N. J. and Beane, W. S. (2009). Regeneration: the origin of cancer or a possible cure? *Semin. Cell Dev. Biol.* **20**, 557-564. doi:10.1016/j.semcdb.2009.04.005

Oviedo, N. J. and Levin, M. (2007). smedinx-11 is a planarian stem cell gap junction gene required for regeneration and homeostasis. *Development* **134**, 3121-3131. doi:10.1242/dev.006635

Oviedo, N. J., Pearson, B. J., Levin, M. and Sánchez Alvarado, A. (2008). Planarian PTEN homologs regulate stem cells and regeneration through TOR signaling. *Dis. Model. Mech.* **1**, 131-143. doi:10.1242/dmm.000117

Oviedo, N., Morokuma, J., Walentek, P., Kema, I. P., Gu, M. B., Ahn, J.-M., Hwang, J. S., Gojobori, T. and Levin, M. (2010). Long-range neural and gap junction protein-mediated cues control polarity during planarian regeneration. *Dev. Biol.* **339**, 188-199. doi:10.1016/j.ydbio.2009.12.012

Pearson, B. J. and Sánchez Alvarado, A. (2010). A planarian p53 homolog regulates proliferation and self-renewal in adult stem cell lineages. *Development* **137**, 213-221. doi:10.1242/dev.044297

Peiris, T. H., Ramirez, D., Barghouth, P. G., Ofoha, U., Davidian, D., Weckerle, F. and Oviedo, N. J. (2016). Regional signals in the planarian body guide stem cell fate in the presence of genomic instability. *Development* **143**, 1697-1709. doi:10.1242/dev.131318

Pellettieri, J., Fitzgerald, P., Watanabe, S., Mancuso, J., Green, D. R. and Sánchez Alvarado, A. (2010). Cell death and tissue remodeling in planarian regeneration. *Dev. Biol.* **338**, 76-85. doi:10.1016/j.ydbio.2009.09.015

Petersen, C. P. and Reddien, P. W. (2008). Smed-betacatenin-1 is required for anteroposterior blastema polarity in planarian regeneration. *Science* **319**, 327-330. doi:10.1126/science.1149943

Petersen, C. P. and Reddien, P. W. (2009). A wound-induced Wnt expression program controls planarian regeneration polarity. *Proc. Natl. Acad. Sci. USA* **106**, 17061-17066. doi:10.1073/pnas.0906823106

Petersen, C. P. and Reddien, P. W. (2011). Polarized notum activation at wounds inhibits Wnt function to promote planarian head regeneration. *Science* **332**, 852-855. doi:10.1126/science.1202143

Pirotte, N., Stevens, A.-S., Fraguas, S., Plusquin, M., Van Roten, A., Van Belleghem, F., Paesen, R., Ameloot, M., Cebrià, F., Artois, T. et al. (2015). Reactive oxygen species in planarian regeneration: an upstream necessity for correct patterning and brain formation. *Oxid. Med. Cell. Longev.* **2015**, 392476. doi:10.1155/2015/392476

Plusquin, M., Stevens, A.-S., Van Belleghem, F., Degheselle, O., Van Roten, A., Vroonen, J., Blust, R., Cuypers, A., Artois, T. and Smeets, K. (2012). Physiological and molecular characterisation of cadmium stress in Schmidtea mediterranea. *Int. J. Dev. Biol.* **56**, 183-191. doi:10.1387/ijdb.113485mp

Pomerantz, J. H. and Blau, H. M. (2013). Tumor suppressors: enhancers or suppressors of regeneration? *Development* **140**, 2502-2512. doi:10.1242/dev.084210

Reddien, P. W. and Sánchez Alvarado, A. (2004). Fundamentals of planarian regeneration. *Annu. Rev. Cell Dev. Biol.* **20**, 20725-20757. doi:10.1146/annurev.cellbio.20.010403.095114

Reddien, P. W., Oviedo, N. J., Jennings, J. R., Jenkin, J. C. and Sánchez Alvarado, A. (2005). SMEDWI-2 is a PIWI-like protein that regulates planarian stem cells. *Science* **310**, 1327-1330. doi:10.1126/science.1116110

Resch, A. M., Palakodeti, D., Lu, Y.-C., Horowitz, M. and Graveley, B. R. (2012). Transcriptome analysis reveals strain-specific and conserved stemness genes in Schmidtea mediterranea. *PLoS ONE* **7**, e34447. doi:10.1371/journal.pone.0034447

Reuter, H., März, M., Vogg, M. C., Eccles, D., Grífol-Boldú, L., Wehner, D., Owlarn, S., Adell, T., Weidinger, G. and Bartscherer, K. (2015). Beta-catenin-dependent control of positional information along the AP body axis in planarians involves a teashirt family member. *Cell Rep.* **10**, 253-265. doi:10.1016/j.celrep.2014.12.018

Reya, T., Duncan, A. W., Ailles, L., Domen, J., Scherer, D. C., Willert, K., Hintz, L., Nusse, R. and Weissman, I. L. (2003). A role for Wnt signalling in self-renewal of haematopoietic stem cells. *Nature* **423**, 409-414. doi:10.1038/nature01593

Riss, J., Khanna, C., Koo, S., Chandramouli, G. V. R., Yang, H. H., Hu, Y., Kleiner, D. E., Rosenwald, A., Schaefer, C. F., Ben-Sasson, S. A. et al. (2006). Cancers as wounds that do not heal: differences and similarities between renal regeneration/repair and renal cell carcinoma. *Cancer Res.* **66**, 7216-7224. doi:10.1158/0008-5472.CAN-06-0040

Rompolas, P., Mesa, K. R. and Greco, V. (2013). Spatial organization within a niche as a determinant of stem-cell fate. *Nature* **502**, 513-518. doi:10.1038/nature12602

Rossi, L., Iacopetti, P. and Salvetti, A. (2012). Stem cells and neural signalling: the case of neoblast recruitment and plasticity in low dose X-ray treated planarians. *Int. J. Dev. Biol.* **56**, 135-142. doi:10.1387/ijdb.123505lr

RStudio Team. (2015). *RStudio: Integrated Development for R*. Boston: RStudio, Inc.

Sahu, S., Dattani, A. and Aboobaker, A. A. (2017). Secrets from immortal worms: what can we learn about biological ageing from the planarian model system? *Semin. Cell Dev. Biol.* **70**, 108-121. doi:10.1016/j.semcdb.2017.08.028

Salvetti, A., Rossi, L., Bonuccelli, L., Lena, A., Pugliesi, C., Rainaldi, G., Evangelista, M. and Gremigni, V. (2009). Adult stem cell plasticity: neoblast repopulation in non-lethally irradiated planarians. *Dev. Biol.* **328**, 305-314. doi:10.1016/j.ydbio.2009.01.029

Schaeffer, D. J., Tehseen, W. M., Johnson, L. R., McLaughlin, G. L., Hassan, A. S., Reynolds, H. A. and Hansen, L. G. (1991). Cocarcinogenesis between cadmium and Aroclor 1254 in planarians is enhanced by inhibition of glutathione synthesis. *Qual. Assur.* **1**, 31-41.

Scimone, M. L., Cote, L. E. and Reddien, P. W. (2017). Orthogonal muscle fibres have different instructive roles in planarian regeneration. *Nature* **551**, 623-628. doi:10.1038/nature24660

Seebeck, F., März, M., Meyer, A.-W., Reuter, H., Vogg, M. C., Stehling, M., Mildner, K., Zeuschner, D., Rabert, F. and Bartscherer, K. (2017). Integrins are required for tissue organization and restriction of neurogenesis in regenerating planarians. *Development* **144**, 795-807. doi:10.1242/dev.139774

Shiroor, D. A., Bohr, T. E. and Adler, C. E. (2019). Injury stimulates stem cells to resist radiation-induced apoptosis. *bioRxiv* doi:10.1101/688168

Sikes, J. M. and Newmark, P. A. (2013). Restoration of anterior regeneration in a planarian with limited regenerative ability. *Nature* **500**, 77-80. doi:10.1038/nature12403

Stevens, A.-S., Willems, M., Plusquin, M., Ploem, J.-P., Winckelmans, E., Artois, T. and Smeets, K. (2017). Stem cell proliferation patterns as an alternative for in vivo prediction and discrimination of carcinogenic compounds. *Sci. Rep.* **7**, 45616. doi:10.1038/srep45616

Stevens, A.-S., Wouters, A., Ploem, J.-P., Pirotte, N., Van Roten, A., Willems, M., Hellings, N., Franken, C., Koppen, G., Artois, T. et al. (2018). Planarians customize their stem cell responses following genotoxic stress as a function of exposure time and regenerative state. *Toxicol. Sci.* **162**, 251-263. doi:10.1093/toxsci/kfx247

Stoker, A. W., Hatier, C. and Bissell, M. J. (1990). The embryonic environment strongly attenuates v-src oncogenesis in mesenchymal and epithelial tissues, but not in endothelia. *J. Cell Biol.* **111**, 217-228. doi:10.1083/jcb.111.1.217

Sundaram, G. M., Quah, S. and Sampath, P. (2018). Cancer: the dark side of wound healing. *FEBS J.* **285**, 4516-4534. doi:10.1111/febs.14586

Sureda-Gómez, M., Martín-Durán, J. M. and Adell, T. (2016). Localization of planarian β-CATENIN-1 reveals multiple roles during anterior-posterior regeneration and organogenesis. *Development* **143**, 4149-4160. doi:10.1242/dev.135152

Swapna, L. S., Molinaro, A. M., Lindsay-Mosher, N., Pearson, B. J. and Parkinson, J. (2018). Comparative transcriptomic analyses and single-cell RNA sequencing of the freshwater planarian Schmidtea mediterranea identify major cell types and pathway conservation. *Genome Biol.* **19**, 124. doi:10.1186/s13059-018-1498-x

Tan, T. C. J., Rahman, R., Jaber-Hijazi, F., Felix, D. A., Chen, C., Louis, E. J. and Aboobaker, A. (2012). Telomere maintenance and telomerase activity are differentially regulated in asexual and sexual worms. *Proc. Natl. Acad. Sci. USA* **109**, 4209-4214. doi:10.1073/pnas.1118885109

Tao, S., Tang, D., Morita, Y., Sperka, T., Omrani, O., Lechel, A., Sakk, V., Kraus, J., Kestler, H. A., Kühl, M. et al. (2015). Wnt activity and basal niche position sensitize intestinal stem and progenitor cells to DNA damage. *EMBO J.* **34**, 624-640. doi:10.15252/embj.201490700

Thiruvalluvan, M., Barghouth, P. G., Tsur, A., Broday, L. and Oviedo, N. J. (2018). SUMOylation controls stem cell proliferation and regional cell death through Hedgehog signaling in planarians. *Cell. Mol. Life Sci.* **75**, 1285-1301. doi:10.1007/s00018-017-2697-4

Tomasetti, C. and Vogelstein, B. (2015). Cancer etiology. Variation in cancer risk among tissues can be explained by the number of stem cell divisions. *Science* **347**, 78-81. doi:10.1126/science.1260825

Umesono, Y., Tasaki, J., Nishimura, Y., Hrouda, M., Kawaguchi, E., Yazawa, S., Nishimura, O., Hosoda, K., Inoue, T. and Agata, K. (2013). The molecular logic for planarian regeneration along the anterior–posterior axis. *Nature* **500**, 73-76. doi:10.1038/nature12359

Vahidi Ferdousi, L., Rocheteau, P., Chayot, R., Montagne, B., Chaker, Z., Flamant, P., Tajbakhsh, S. and Ricchetti, M. (2014). More efficient repair of DNA

double-strand breaks in skeletal muscle stem cells compared to their committed progeny. *Stem Cell Res.* **13**, 492-507. doi:10.1016/j.scr.2014.08.005

Van Roten, A., Barakat, A. Z. A.-Z., Wouters, A., Tran, T. A., Mouton, S., Noben, J.-P., Gentile, L. and Smeets, K. (2018). A carcinogenic trigger to study the function of tumor suppressor genes in Schmidtea mediterranea. *Dis. Model. Mech.* **11**, dmm032573. doi:10.1242/dmm.032573

van Wolfswinkel, J. C., Wagner, D. E. and Reddien, P. W. (2014). Single-cell analysis reveals functionally distinct classes within the planarian stem cell compartment. *Cell Stem Cell* **15**, 326-39. doi:10.1016/j.stem.2014.06.007

Vitale, I., Manic, G., De Maria, R., Kroemer, G. and Galluzzi, L. (2017). DNA damage in stem cells. *Mol. Cell* **66**, 306-319. doi:10.1016/j.molcel.2017.04.006

Voura, E. B., Montalvo, M. J., Dela Roca,, K. T., Fisher, J. M., Defamie, V., Narala, S. R., Khokha, R., Mulligan, M. E. and Evans, C. A. (2017). Planarians as models of cadmium-induced neoplasia provide measurable benchmarks for mechanistic studies. *Ecotoxicol. Environ. Saf.* **142**, 544-554. doi:10.1016/j.ecoenv.2017.04.044

Wagner, D. E., Wang, I. E. and Reddien, P. W. (2011). Clonogenic neoblasts are pluripotent adult stem cells that underlie planarian regeneration. *Science* **332**, 811-816. doi:10.1126/science.1203983

Wagner, D. E., Ho, J. J. and Reddien, P. W. (2012). Genetic regulators of a pluripotent adult stem cell system in planarians identified by RNAi and clonal analysis. *Cell Stem Cell* **10**, 299-311. doi:10.1016/j.stem.2012.01.016

Wenemoser, D. and Reddien, P. W. (2010). Planarian regeneration involves distinct stem cell responses to wounds and tissue absence. *Dev. Biol.* **344**, 979-991. doi:10.1016/j.ydbio.2010.06.017

Witchley, J. N., Mayer, M., Wagner, D. E., Owen, J. H. and Reddien, P. W. (2013). Muscle cells provide instructions for planarian regeneration. *Cell Rep.* **4**, 633-641. doi:10.1016/j.celrep.2013.07.022

Zeng, A., Li, H., Guo, L., Gao, X., McKinney, S., Wang, Y., Yu, Z., Park, J., Semerad, C., Ross, E. et al. (2018). Prospectively isolated Tetraspanin^{+} neoblasts are adult pluripotent stem cells underlying planaria regeneration. *Cell* **173**, 1593-1608.e20. doi:10.1016/j.cell.2018.05.006

Zhang, D.-Y., Wang, H.-J. and Tan, Y.-Z. (2011). Wnt/beta-catenin signaling induces the aging of mesenchymal stem cells through the DNA damage response and the p53/p21 pathway. *PLoS ONE* **6**, e21397. doi:10.1371/journal.pone.0021397

Zhao, Y., Yi, J., Tao, L., Huang, G., Chu, X., Song, H. and Chen, L. (2018). Wnt signaling induces radioresistance through upregulating HMGB1 in esophageal squamous cell carcinoma. *Cell Death Dis.* **9**, 433. doi:10.1038/s41419-018-0466-4

Zilakos, N. P., Zafiratos, C. S. and Parchment, R. E. (1996). Stage-dependent genetically-based deformities of the regenerating newt limb from 4-nitroquinoline-N-oxide mutagenesis: potential embryonic regulation of cancer. *Differentiation* **60**, 67-74. doi:10.1046/j.1432-0436.1996.6020067.x